A 1 100 years of scattering and beyond

Th. Brückel
Jülich Centre for Neutron Science
Forschungszentrum Jülich GmbH

Contents

Lecture Notes of the 43rd IFF Spring School "Scattering Methods for Condensed Matter Research: Towards Novel Applications at Future Sources" (Forschungszentrum Jülich, 2012).

1 A brief history of x-ray and neutron scattering

"If I have seen further it is by standing on the shoulders of giants.
(Sir Isaac Newton, 1643 - 1727)".

A discovery made exactly 100 years ago revolutionized mankinds' understanding of condensed matter: the observation of interference patterns obtained with x-rays scattered by a single crystal [1]. In 1914 Max von Laue received the Nobel prize in physics for the interpretation of these observations (figure 1).

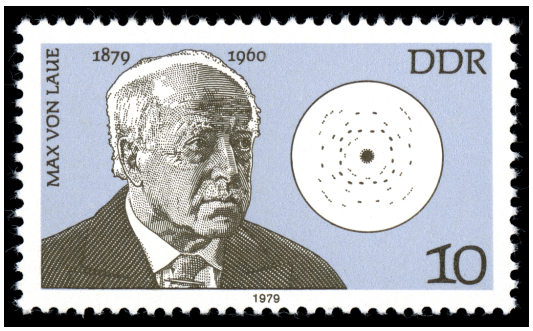

Fig. 1: *Max von Laue and a Laue diffraction pattern on a stamp from the former German Democratic Republic DDR.*

One cannot overestimate the impact of this discovery: it was the first proof that atoms as the elementary building blocks of condensed matter are arranged in a periodic manner within a crystal; at the same time the experiment proved the wave nature of x-rays. The importance of x-ray diffraction for condensed matter research was immediately recognized at the beginning of the 20th century as evidenced by the award of two successive Nobel prizes in physics, one 1914 to Max von Laue "*for his discovery of the diffraction of x-rays by crystals*" and a second one 1915 to William and Lawrence Bragg "*for their services in the analysis of crystal structure by means of x-rays*" [2]. Both, Laue and the Bragg's, could build on earlier experiments by Geiger and Marsden [3, 4] and interpretated by Ernest Rutherford [5] which proved - again by scattering, this time with alpha particles, - that the atom was composed of a nucleus with a diameter in the femtometer (10^{-15} m) range, while the surrounding electron cloud has a typical extension of 1 Å = 0.1 nm = 10^{-10} m. While this seems trivial to us nowadays, this was a breakthrough discovery at the time since alternate models for the atomic structure with a more continuous distribution of positive and negative charges had been discussed and only scattering methods could provide the final proof of the now well accepted structure of the atom consisting of a tiny nucleus and an extended electron cloud. Since these early experiments, a lot of scattering investigations on condensed matter systems have been done. The overwhelming part of our present-day knowledge of the atomic structure of condensed matter is based on x-ray structure investigations, complemented by electron and neutron diffraction. Electrons due to the strong Coulomb interaction with the atoms suffer

multiple scattering events, which make a quantitative evaluation to obtain atomic positions much more difficult. As a probe in condensed matter, electrons made their impact mainly with microscopy techniques (see lecture F 1 by Rafal Dunin-Borkowski). Ernst Ruska was awarded the Nobel prize in physics in 1986 "*for the design of the first electron microscope*".

Entirely new possibilities became apparent with the discovery of the neutrons by James Chadwick [6, 7]. He received the Nobel prize in physics in 1935. However, for neutrons to become a valuable probe in condensed matter research, they had to be available in large quantities as free particles. This was only possible with the advent of nuclear reactors, where nuclear fission is sustained as a chain reaction. The first man-made nuclear reactor, Chicago Pile-1, was built beneath the west stands of Stagg Field, a former squash rackets court of the campus of the University of Chicago. The reactor went critical on December 2, 1942. The experiment was lead by Enrico Fermi, an Italian physicist, who was awarded the Nobel prize in physics in 1938 for this work on transuranium elements. The reactor was a rather crude construction based on a cubical lattice of graphite and uranium oxide blocks. It had no provision for cooling, but two rudimentary manual emergency shutdown systems: one man to cut with an axe a rope, on which a neutron absorbing cadmium rod was suspended, which would drop into the reactor and stop the chain reaction; and a team of three guys standing above the pile ready to flood it with a cadmium salt solution. Considering what was known about nuclear fission at the time it is no wonder that the standing joke among the scientists working there was: *if people could see what we are doing with a million and a half of their dollars, they would think we are crazy. If they knew, why we are doing it, they would know we are [8]*. Out of this very crude first experiment, which was only possible within the World War II Manhattan Project, the modern sophisticated research reactors with their extremely high safety standards developed. In contrast to their big brothers, the nuclear power plants, these reactors are mainly used for isotope production and neutron scattering experiments. The two pioneers of neutron diffraction and inelastic neutron scattering, Clifford G. Shull and Bertram M. Brockhouse, respectively, received the Nobel prize in physics in 1994, many years after the first neutron diffraction experiments, which were performed at Oak Ridge National Lab in 1946. The work of Clifford Shull clearly demonstrated the different contrast mechanisms of neutron scattering compared to x-ray scattering, which in particular allows one to make light elements like hydrogen visible and to distinguish different isotopes like hydrogen and deuterium [9]. But Shull also demonstrated that neutrons, due to their nuclear magnetic moment, could not only be used to determine the arrangement of atoms in solids but they could also be used to determine the magnetic structure e.g. of antiferromagnetic materials [10]. While Shull studied "*where the atoms are located*" and eventually how the magnetic moments are arranged in the solid, Brockhouse observed for the first time "*how the atoms are moving*" in the solid. He developed the so-called triple-axis spectroscopy, which enables the determination of the dispersion relations of lattice vibrations and spin waves [11].

Since the early work in x-ray and neutron scattering sketched above, many years have passed, new radiation sources such as synchrotron radiation sources or neutron spallation sources have been developed, experimental methods and techniques have been refined and the corresponding theoretical concepts developed. For the further development of modern condensed matter research, the availability of these probes to study the structure and

dynamics on a microscopic level is absolutely essential. It comes as no surprise therefore that scattering methods have been employed in ground-breaking work which lead to recent Nobel prizes. The most recent example is the Nobel prize in chemistry 2011, which was awarded to Dan Shechtman "*for the discovery of quasi-crystals*". By means of electron diffraction, Shechtman discovered icosahedral symmetry in aluminum manganese alloys. The observed tenfold symmetry is not compatible with translational symmetry in three dimensions. While the icosahedral symmetry was discovered with electron diffraction, the question where the atoms are located requires the collection of many weak quasicrystal reflections and the analysis of their intensities, which is only possible with x-ray and neutron diffraction. A higher dimensional reciprocal space approach had to be developed to explain the diffraction pattern of such quasicrystals. Another outstanding piece of work in x-ray diffraction is the Nobel prize in chemistry 2009, which was awarded jointly to Venkatraman Ramakrishnan, Thomas A. Steitz and Ada E. Yonath "*for studies of the structure and function of the ribosome*". Ribosomes translate DNA information into life by producing proteins, which in turn control the chemistry in all living organisms. By means of x-ray crystallography the Nobel awardees were able to map the position for each and everyone of the hundreds of thousands of atoms that make up the ribosome. 3D models that show how different antibiotics bind to the ribosome are now used by scientists in order to develop new drugs.

On occasion of the 100 years anniversary of the discovery of x-ray diffraction from single crystals, we have given a brief and absolutely incomplete historical summary of the development of scattering methods. This Spring School is devoted to modern applications of this powerful tool. In this introductory overview, we will now give a short summary of which information we can obtain from scattering experiments, compare the two probes x-rays and neutrons briefly, discuss techniques and applications, giving an outlook into the bright future of the field which the two new European facilities promise: the European X-Ray Free Electron Laser X-FEL (www.xfel.eu) and the European Spallation Source ESS (www.ess-scandinavia.eu) and finally explain how large-scale facilities for this type of research are organized.

2 Introduction to scattering

2.1 Scattering - a critical tool for science

Scattering is the physical process in which radiation or moving particles are being deflected by an object from straight propagation. If the energy or wavelength of the scattered particles or waves, respectively, is the same as before the scattering process, one speaks of elastic scattering or diffraction, otherwise of inelastic scattering. The analysis of the energy of the scattered radiation with respect to the energy of the incident radiation is called spectroscopy.

Nearly all information which we humans as individuals collect on a day-to-day basis about the world in which we live, comes from light scattering and imaging through our eyes. It is only natural that scientists mimic this process of obtaining information in well controlled scattering experiments: they build a source of radiation, direct a beam of towards a sample,

detect the radiation scattered from a sample, i. e. convert the signal into an electronic signal, which they can then treat with computers. In most cases one wants an undisturbed image of the object under investigation and therefore chooses the radiation, so that it does not influence or modify the sample. Scattering is therefore a non-destructive and very gentle method, if the appropriate type of radiation is chosen for the experiment.

What other requirements must the radiation fulfill to be useful for scattering experiments? In condensed matter science we want to go beyond our daily experience and understand the microscopic atomic structure of matter, i. e. we want to find out where the atoms are located inside our samples and also how they move. This cannot be done by light scattering. Why? Well, in general light is scattered from the surface and does not penetrate enough into many materials, such as metals for example. On the other hand, if it penetrates like in the case of glass it is normally just being transmitted except if we have a very bad glass with lots of inhomogeneities. But the main reason is actually that light has a too long wavelength. It is quite intuitive to understand that if we want to measure the distance between the atoms, we need a "ruler" of comparable lengths. The distance between atoms is in the order of 0.1 nm = 10^{-10} m = 0.0000000001 m. Since the distance between atoms is such an important length scale in condensed matter science, it has been given its own unit: 0.1 nm = 1 Ångstrøm = 1 Å. If we compare the wavelength of light with this characteristic length scale, it is 4000 to 7000 times longer and therefore not appropriate to measure distances between atoms. In the electromagnetic spectrum, x-rays have a well adapted wavelength of about 1 Å for studies on such a microscopic scale. They also have a large penetration power as everybody knows from the medical x-ray images.

It should be pointed out that scattering is a much more general method in science, which is not only used by condensed matter scientists. Examples include:

- in the geosciences, seismological studies of the propagation and deflection of elastic waves through the earth are the primary tool for underground exploration (e.g. to detect petroleum bearing formations) and the mapping of the earth's interior.
- the scattering of radar waves is being used e.g. for air traffic control or the detection of weather formations.
- nuclear- and particle physics uses the scattering of high energy elementary particles (electrons, protons etc.) from accelerators to investigate the structure of the nuclei or nucleons etc.

2.2 Scattering cross section

Lets look at a scattering experiment in condensed matter science in the so-called *Fraunhofer- or far-field-approximation*, where we assume that the incident and scattered waves can be described as plane waves with wavelengths λ and λ' (strictly monochromatic) and propagation direction $\hat{\underline{k}}$ and $\hat{\underline{k}}'$, respectively[1]. Let us define the so-called *scattering vector*

[1] Vector quantities are labeled by underlining. Unit vectors are marked by a circumflex ^.

$$\underline{Q} = \underline{k}' - \underline{k} \tag{1}$$

where $\underline{k}$ and $\underline{k}'$ are the wave vectors of the incident and scattered radiation, respectively:

$$\underline{k} = \hat{\underline{k}} \cdot \frac{2\pi}{\lambda};\ \underline{k}' = \hat{\underline{k}}' \cdot \frac{2\pi}{\lambda'} \tag{2}$$

$\hbar\underline{Q}$ represents the momentum transfer during scattering, since according to de Broglie, the momentum of the particle corresponding to the wave with wave vector $\underline{k}$ is given by $\underline{p}=\hbar\underline{k}$. The magnitude of the scattering vector can be calculated from wavelength λ and scattering angle 2θ (between $\underline{k}$' and $\underline{k}$) as follows

$$Q = \left|\underline{Q}\right| = \sqrt{k^2 + k'^2 - 2kk'\cos 2\theta} \Rightarrow Q = \frac{4\pi}{\lambda}\sin\theta \tag{3}$$

A scattering experiment comprises the measurement of the intensity distribution as a function of the scattering vector. The scattered intensity is proportional to the so-called *cross section*, where the proportionality factors arise from the detailed geometry of the experiment. For a definition of the scattering cross section, we refer to Figure 2.

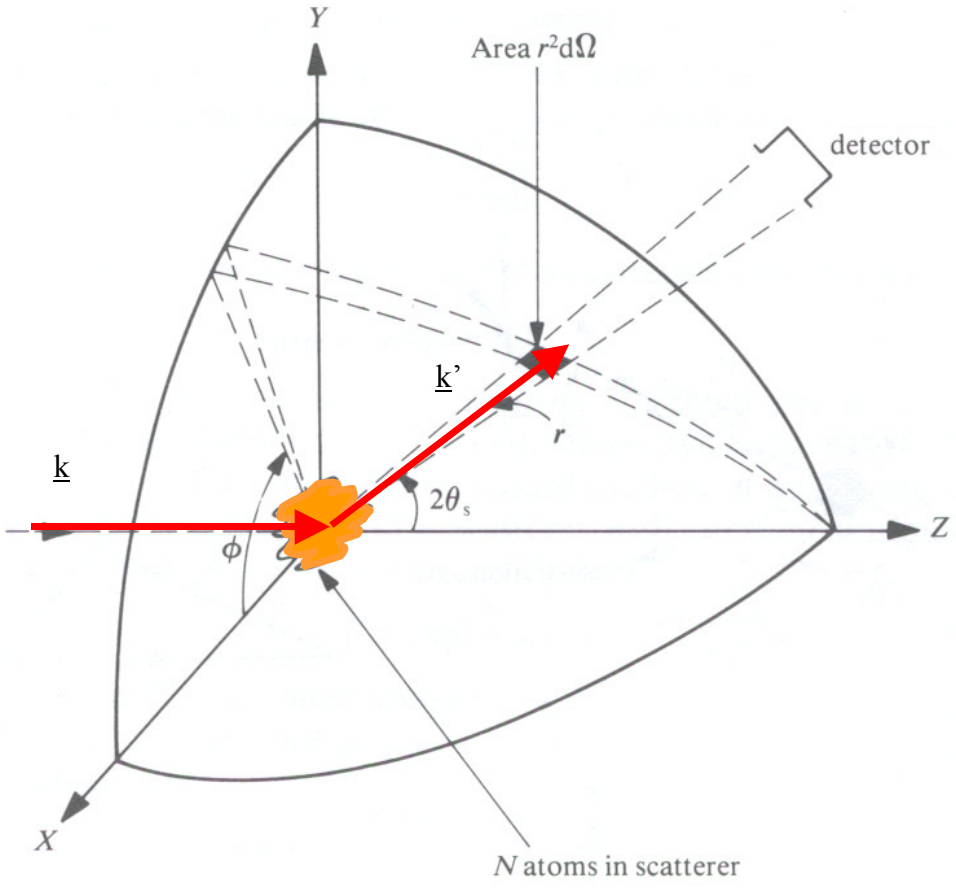

Fig. 2: *Geometry used for the definition of the scattering cross section.*

If n' particles are scattered per second into the solid angle $d\Omega$ seen by the detector under the scattering angle 2θ and into the energy interval between E' and $E' + dE'$, then we can define the so-called *double differential cross section* by:

$$\frac{d^2\sigma}{d\Omega dE'} = \frac{n'}{j d\Omega dE'} \tag{4}$$

Here j refers to the incident beam flux in terms of particles per area and time. If we are not interested in the change of the energy of the radiation during the scattering process, or if our detector is not able to resolve this energy change, then we will describe the angular dependence by the so-called *differential cross section:*

$$\frac{d\sigma}{d\Omega} = \int_0^\infty \frac{d^2\sigma}{d\Omega dE'} dE' \tag{5}$$

Finally the so-called *total scattering cross section* gives us a measure for the total scattering probability independent of changes in energy and scattering angle:

$$\sigma = \int_0^{4\pi} \frac{d\sigma}{d\Omega} d\Omega \tag{6}$$

For a diffraction experiment, our task is to determine the arrangement of the atoms in the sample from the knowledge of the scattering cross section $d\sigma / d\Omega$. The relationship between scattered intensity and the structure of the sample is particularly simple in the so-called *Born approximation*, which is often also referred to as *kinematic scattering approximation* (see lecture A2). In this case, refraction of the beam entering and leaving the sample, multiple scattering events and the extinction of the primary beam due to scattering within the sample are being neglected (these effects will be dealt with in lecture A3). Following Figure 3, the phase difference between a wave scattered at the origin of the coordinate system and at position $\underline{r}$ is given by

$$\Delta\Phi = 2\pi \cdot \frac{\left(\overline{AB} - \overline{CD}\right)}{\lambda} = \underline{k}' \cdot \underline{r} - \underline{k} \cdot \underline{r} = \underline{\underline{Q}} \cdot \underline{r} \tag{7}$$

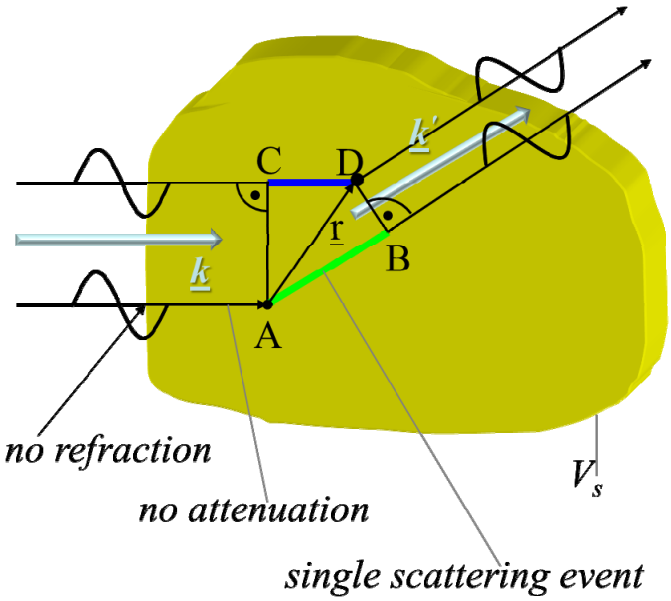

Fig. 3: *A sketch illustrating the phase difference between a beam scattered at the origin of the coordinate system and a beam scattered at the position r. The yellow body represents the sample from which we scatter.*

The probability for a scattering event to occur at position $\underline{r}$ is proportional to the local interaction potential $V(\underline{r})$ between radiation and sample. For a coherent scattering event (interference of scattered waves), the total scattering amplitude is given by a linear superposition of the waves scattered from all points within the sample volume V_s, i.e. by the integral

$$A(\underline{Q}) \sim \int_{V_{\underline{s}}} V(\underline{r}) \cdot e^{i\underline{Q}\cdot\underline{r}} d^3r \tag{8}$$

This equation demonstrates that the scattered amplitude is directly connected to the interaction potential by a simple Fourier transform: *scattering is a probe in reciprocal space, not in direct space and gives direct access to thermodynamic ensemble averages!*

A knowledge of the scattering amplitude for all scattering vectors $\underline{Q}$ allows us to determine via a Fourier transform the interaction potential uniquely. This is the complete information on the sample, which can be obtained by the scattering experiment. Unfortunately nature is not so simple. On one hand, there is the more technical problem that one is unable to determine the scattering cross section for <u>all</u> values of momentum transfer $\hbar\underline{Q}$. The more fundamental problem, however, is given by the fact that normally the amplitude of the scattered wave is not measurable. Instead only the scattered intensity

$$I(Q) \sim \left|A(Q)\right|^2 \tag{9}$$

can be determined. Therefore the phase information is lost and the simple reconstruction of the scattering potential via a Fourier transform is no longer possible. This is the so-called *phase problem* of scattering. There are ways to overcome the phase problem, i.e. by the use of reference waves. Then the potential $V(\underline{r})$ becomes directly accessible. The question, which information we can obtain from a scattering experiment despite the phase problem, will be addressed below and in subsequent lectures.

Which wavelength do we have to choose to obtain the required real space resolution? For information on a length scale L, a phase difference of about $Q \cdot L \approx 2\ \pi$ leads from the primary beam $(Q = 0)$ to the interference maximum. According to (3) $Q \approx 2\pi/\lambda$ for practical scattering angles $(2\theta \sim 60°)$. Combining these two estimates, we end up with the requirement that the wavelength λ has to be in the order of the real space length scale L under investigation. To give an example: with the wavelength in the order of *0.1 nm*, atomic resolution can be achieved in a scattering experiment.

2.3 Coherence

In the above derivation, we assumed plane waves as initial and final states. For a real scattering experiment, this is an unphysical assumption. In the incident beam, a wave packet is produced by collimation (defining the direction of the beam) and monochromatization (defining the wavelength of the incident beam). Neither the direction $\hat{\underline{k}}$, nor the wavelength λ have sharp values but rather have a distribution of finite width about their respective mean values. This wave packet can be described as a superposition of plane waves. As a consequence, the diffraction pattern will be a superposition of patterns for different incident wave vectors $\underline{k}$ and the question arises, which information is lost due to these non-ideal conditions. This *instrumental resolution* is intimately connected with the *coherence* of the beam. Coherence is needed, so that the interference pattern is not significantly destroyed. Coherence requires a phase relationship between the different components of the beam. Two types of coherence can be distinguished.

- *Temporal or longitudinal coherence* due to a wavelength spread.

A measure for the longitudinal coherence is given by the length, on which two components of the beam with largest wavelength difference (λ and $\lambda+\Delta\lambda$) become fully out of phase. According to the following figure, this is the case for $l_{\parallel} = n \cdot \lambda = \left(n - \frac{1}{2} \right)\left(\lambda + \Delta\lambda \right)$.

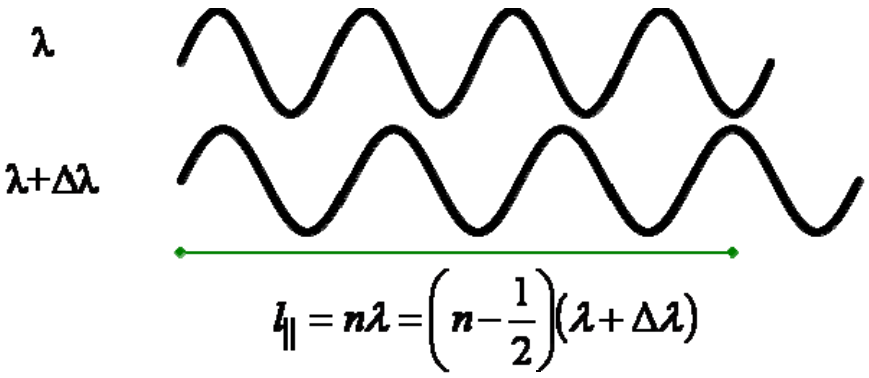

Fig. 4: *A sketch illustrating the longitudinal coherence due to a wavelength spread.*

From this, we obtain the *longitudinal coherence length* $l_{\parallel}$ as

$$l_{\parallel} = \frac{\lambda^2}{2\Delta\lambda} \tag{10}$$

• *Transversal coherence* due to source extension
Due to the extension of the source (transverse beam size), the phase relation is destroyed for large source size or large divergence. According to the following figure, a first minimum occurs for $\frac{\lambda}{2} = d \cdot \sin\theta \approx d \cdot \theta$.

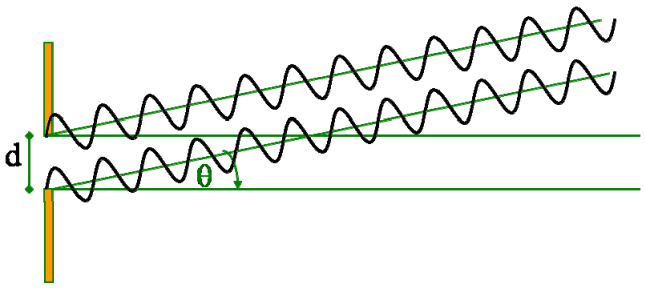

Fig. 5: *A sketch illustrating the transverse coherence due to source extension.*

From this, we obtain the *transversal coherence length* $l_{\perp}$ as

$$l_{\perp} = \frac{\lambda}{2\Delta\theta} \tag{11}$$

Here $\Delta\theta$ is the divergence of the beam. Note that $l_{\perp}$ can be different along different spatial directions: in many instruments, the vertical and horizontal collimations are different.

Together, the longitudinal and the two transversal coherence lengths (in two directions perpendicular to the beam propagation) define a *coherence volume*. This is a measure for a volume within the sample, in which the amplitudes of all scattered waves superimpose to produce an interference pattern. Normally, the coherence volume is significantly smaller than the sample size, typically a few *100 Å* for neutron scattering, up to *μm* for synchrotron

radiation. Scattering between different coherence volumes within the sample is no longer coherent, i. e. instead of the amplitudes, the intensities of the waves contributing to the scattering pattern have to be added. This limits the real space resolution of a scattering experiment to the extension of the coherence volume.

2.4 Pair correlation functions

After having clarified the conditions under which we can expect a coherent scattering process, let us now come back to the question, which information is accessible from the intensity distribution of a scattering experiment. From (9) we see that the phase information is lost during the measurement of the intensity. For this reason the Fourier transform of the scattering potential is not directly accessible in most scattering experiments (note however that phase information can be obtained in certain cases).

Substituting (8) into (9) and applying variable substitution $\underline{R}=\underline{r}'-\underline{r}$, we obtain for the magnitude square of the scattering amplitude, a quantity directly accessible in a diffraction experiment:

$$I(Q) \sim \left| A\left(\underline{Q}\right)\right|^2 \sim \int_{V_S} d^3r' V(\underline{r}') e^{i\underline{Q}\cdot\underline{r}'} \int_{V_S} d^3r V^*(\underline{r}) e^{-i\underline{Q}\cdot\underline{r}} = \iint_{V_S} d^3r' d^3r\, V\left(\underline{r}\right) V^*(\underline{r}') e^{i\underline{Q}\cdot(\underline{r}'-\underline{r})}$$
$$= \iint_{V_S} d^3R d^3r\, V\left(\underline{R}+\underline{r}\right) V^*(\underline{r}) e^{i\underline{Q}\cdot\underline{R}} \qquad (12)$$

This function denotes the so-called *Patterson function* in crystallography or more general the *static pair correlation function:*

$$P\left(\underline{R}\right) = \int_{Vs} d^3r V^*(\underline{r}) V(\underline{r}+\underline{R}) \qquad (13)$$

$P(\underline{R})$ correlates the value of the scattering potential at position $\underline{r}$ with the value at the position $\underline{r}+\underline{R}$, integrated over the entire sample volume V_s. If, averaged over the sample, no correlation exists between the values of the scattering potentials at position $\underline{r}$ and $\underline{r}+\underline{R}$, then the Patterson function $P(\underline{R})$ vanishes. If, however, a periodic arrangement of a pair of atoms exists in the sample with a difference vector $\underline{R}$ between the positions, then the Patterson function will have an extremum for this vector $\underline{R}$. Thus in a periodic arrangement the Patterson function reproduces all the vectors connecting one atom with another atom.

As will be shown in detail in lecture A5, pair correlation functions are being determined quite generally in a scattering experiment. In a coherent inelastic scattering experiment, we measure a cross section proportional to the *scattering law* $S(\underline{Q},\omega)$, which is the Fourier transform with respect to space and time of the spatial and temporal pair correlation function:

$$\frac{d^2\sigma}{d\omega d\Omega} \sim S\left(\underline{Q},\omega\right) = \frac{1}{2\pi\hbar} \int_{-\infty}^{+\infty} dt\, e^{-i\omega t} \int_{V_S} d^3r e^{i\underline{Q}\underline{r}} G(\underline{r},t) \qquad (14)$$

While the proportionality factor between the double differential cross section and the scattering law depends on the type of radiation and its specific interaction potential with the

system studied, the spatial and temporal pair correlation function is only a property of the system studied and independent of the probe used:

$$G(\underline{r},t)=\frac{1}{N}\sum_{ij}\int_{Vs}d^3r'\left\langle\delta\left(\underline{r}'-\underline{r}_j(0)\right)\cdot\delta\left(\underline{r}'+\underline{r}-\underline{r}_i(t)\right)\right\rangle=\frac{1}{N}\int_{Vs}d^3r'\left\langle\rho\left(\underline{r}',0\right)\rho\left(\underline{r}'+\underline{r},t\right)\right\rangle \quad (15)$$

Here, the pair correlation function is once expressed as a correlation between the position of N point-like particles (expressed by the delta functions) and once by the correlation between the densities at different positions in the sample for different times. In a magnetic system, radiation is scattered from the atomic magnetic moments, which are vector quantities. Therefore, the scattering law becomes a tensor - the Fourier transform of the *spin pair correlations*:

$$\mathbf{S}^{\alpha\beta}(\underline{Q},\omega)=\frac{1}{2\pi}\sum_{l}\int dt\, e^{i\left[\underline{Q}(\underline{R}_l-\underline{R}_0)-\omega t\right]}\left\langle S_0^{\alpha}(0)S_l^{\beta}(t)\right\rangle \quad (16)$$

α, β denote the Cartesian coordinates *x, y, z;* $\underline{R}_0$ and $\underline{R}_l$ are the spatial coordinates of a reference spin *0* and a spin *l* in the system.

2.5 Scattering from a periodic lattice in three dimensions

We now are ready to understand the famous first diffraction experiment by Laue et al. As an example for the application of (8) and (9), we will now discuss the scattering from a three dimensional lattice of point-like scatterers. As we will see later, this situation corresponds to the scattering of thermal neutrons from a single crystal. More precisely, we will restrict ourselves to the case of a Bravais lattice with one atom at the origin of the unit cell. To each atom we attribute a "scattering length b" (see interaction potential of neutrons below). The single crystal is finite with *N, M* and *P* periods along the basis vectors $\underline{a}$, $\underline{b}$ and $\underline{c}$. The scattering potential, which we have to use in (8) is a sum over δ-functions for all scattering centers:

$$V(\underline{r})=\sum_{n=0}^{N-1}\sum_{m=0}^{M-1}\sum_{p=0}^{P-1}b\cdot\delta\left(\underline{r}-\left(n\cdot\underline{a}+m\cdot\underline{b}+p\cdot\underline{c}\right)\right) \quad (17)$$

The scattering amplitude is calculated as a Fourier transform:

$$A\left(\underline{Q}\right)\sim b\sum_{n=0}^{N-1}e^{in\underline{Q}\cdot\underline{a}}\sum_{m=0}^{M-1}e^{im\underline{Q}\cdot\underline{b}}\sum_{p=0}^{P-1}e^{ip\underline{Q}\cdot\underline{c}} \quad (18)$$

Summing up the geometrical series, we obtain for the scattered intensity:

$$I\left(\underline{Q}\right)\sim\left|A\left(\underline{Q}\right)\right|^2=\left|b\right|^2\cdot\frac{\sin^2\frac{1}{2}N\underline{Q}\cdot\underline{a}}{\sin^2\frac{1}{2}\underline{Q}\cdot\underline{a}}\cdot\frac{\sin^2\frac{1}{2}M\underline{Q}\cdot\underline{b}}{\sin^2\frac{1}{2}\underline{Q}\cdot\underline{b}}\cdot\frac{\sin^2\frac{1}{2}P\underline{Q}\cdot\underline{c}}{\sin^2\frac{1}{2}\underline{Q}\cdot\underline{c}} \quad (19)$$

The dependence on the scattering vector $\underline{Q}$ is given by the so-called *Laue function* (19), which factorizes according to the three directions in space. One factor along one lattice direction $\underline{a}$ is plotted in Figure 6.

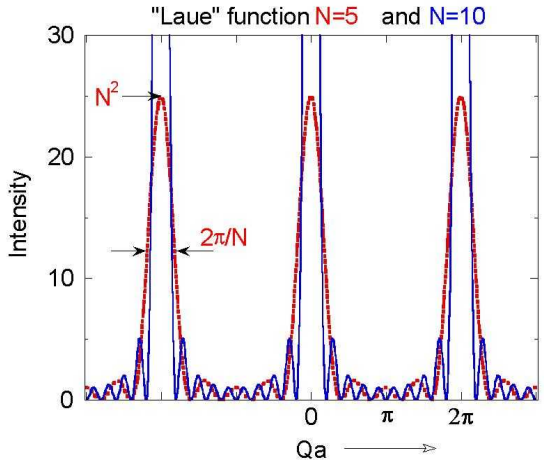

Fig. 6: *Laue function along the lattice direction a for a lattice with five and ten periods, respectively.*

The main maxima occur at the positions $Q = n \cdot 2\pi/a$. The maximum intensity scales with the square of the number of periods N^2, the half width is given approximately by $\Delta Q = 2\pi/(N \cdot a)$. The more periods contribute to coherent scattering, the sharper and higher are the main peaks. Between the main peaks, there are *N-2* side maxima. With increasing number of periods *N*, their intensity becomes rapidly negligible compared to the intensity of the main peaks. The main peaks are of course the well known *Bragg reflections*, which we obtain for scattering from a crystal lattice. From the position of these Bragg peaks in momentum space, the metric of the unit cell can be deduced (lattice constants *a, b, c* and unit cell angles α, β, γ). The width of the Bragg peaks is determined by the size of the coherently scattering volume (parameters *N, M,* and *P*) - and some other factors for real experiments (resolution, mosaic distribution, internal strains, ...).

Via the so-called Ewald construction, it can be shown that the Laue conditions for interference maxima to occur $\underline{Q} \cdot \underline{a} = n \cdot 2\pi$ etc. are equivalent to the *Bragg equation* for scattering from lattice planes (hkl) with interplanar spacings d_{hkl}:

$$2d_{hkl} \sin\theta_{hkl} = \lambda \tag{20}$$

3 X-rays and Neutrons

Since the first scattering experiments, some standard probes for condensed matter research have emerged, which optimally fulfill the requirements for a suitable type of radiation.

First of all, electromagnetic radiation governed by the Maxwell equations can be used. Depending on the resolution requirements, X-rays with wavelength λ about 0.1 nm are being used to achieve atomic resolution, or visible light (λ ~ 350 - 700 nm) is employed to

investigate e. g. colloidal particles in solution. Besides electromagnetic radiation, particle waves can be utilized. It turns out that thermal neutrons with a wavelength $\lambda \sim 0.1$ nm are particularly well adapted to scattering experiments in condensed matter research. Neutrons are governed by the Schrödinger equation of quantum mechanics. An alternative is to use electrons, which for energies of around 100 keV have wavelengths in the order of 0.005 nm. As relativistic particles, they are governed by the Dirac equation. The big drawback of electrons is the strong Coulomb interaction with the electrons in the sample. Therefore neither absorption, nor multiple scattering effects can be neglected. However the abundance of free electrons and the relative ease to produce optical elements makes them very suitable for imaging purposes (electron microscopy). Electrons, but likewise atomic beams, are also very powerful tools for surface science: due to their strong interaction with matter, both types of radiation are very surface sensitive. Low Energy Electron Diffraction LEED and Reflection High Energy Electron Diffraction RHEED are both used for in-situ studies of the crystalline structure during thin film growth, e.g. with Molecular Beam Epitaxy MBE. In what follows we will concentrate on the two probes, which are best suited for bulk studies on an atomic scale: x-rays and neutrons. We will touch upon the radiation sources, briefly discuss the main interaction processes and finally give a comparison of these probes.

3.1 X-ray Sources

Since the early days of Conrad Röntgen X-rays are being produced in the laboratory in sealed vacuum tubes, where electrons from a cathode are accelerated towards the anode. There characteristic- and/or bremsstrahlungradiation is produced. Radiation emitted from such x-ray tubes has been widely used for structural studies in condensed matter science. However, in 1947 a new type of radiation was discovered in a General Electric synchrotron accelerator [12]. It soon turned out that this so-called *synchrotron radiation* has superb properties, see figure 7.

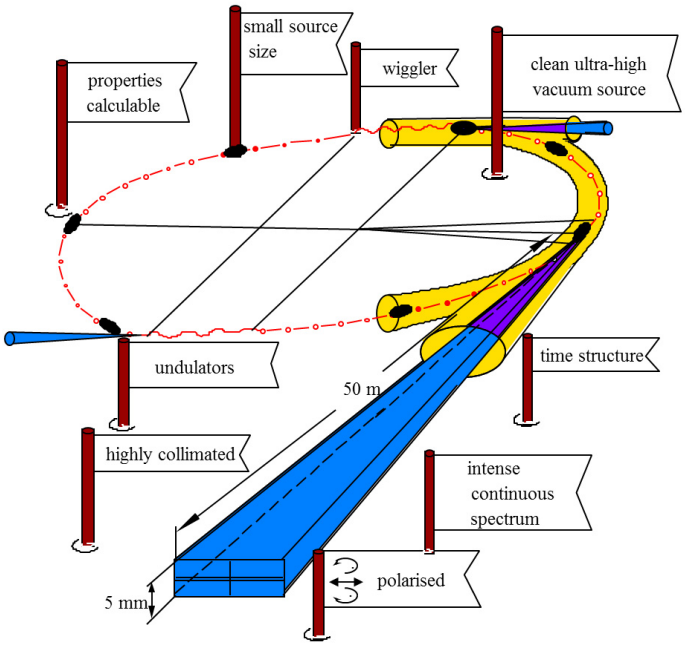

Fig. 7: *Sketch of a synchrotron radiation source indicating the properties of synchrotron radiation.*

Synchrotron radiation is emitted when relativistic charged particles (electrons or positrons) are being accelerated perpendicular to their direction of motion by an appropriate magnetic field. This happens is so-called bending magnets within circular accelerators and this type of radiation has originally been used by solid state physicists in a parasitic mode at particle physics facilities (first generation of synchrotron radiation sources). Second generation synchrotron radiation sources were dedicated to the production of synchrotron radiation, mainly from such bending magnets. However, even more intense radiation can be produced in straight sections of the accelerator by so-called insertion devices - wigglers and undulators - which consist of arrays of magnets with alternating field direction. Modern synchrotron radiation sources of the 3rd generation employ mainly these insertion devices as radiation sources, see lecture C2. This continuous improvement of the source parameters led to an exponential growth of the brilliance, i.e. the spectral photon flux, normalized to the size and divergence of the beam. A further increase of the peak brilliance can be achieved with *free electron lasers*. For the X-ray regime these are based on the SASE principle: *Self Amplified Spontaneous Emission*. In such facilities, an electron beam from a linear accelerator passes through an undulator structure, where synchrotron radiation is produced. The electromagnetic interaction between this radiation and the electron beam travelling in parallel leads to an amplification of the radiation, giving rise to extremely brilliant fully coherent x-ray flashes of about 100 fs duration. Close to DESY in Hamburg such a facility, the *European XFEL* is currently under construction [13]. Details will be presented in lecture C8 by the XFEL managing director, Massimo Altarelli. The facility will open entirely new perspectives for research, see lecture D10 by Henry Chapman.

3.2 Neutron Sources

While neutrons are everywhere - without neutrons we would not exist - they are extremely difficult to produce as free particles, not bound in nuclei. Free neutrons are produced by nuclear physics reactions, which require rather large and high-tech installations. Two main routes to produce free neutrons are being followed today (see figure 8 and lecture C1):

(1) ***Fission*** of the uranium 235 nuclei in a chain reaction; this process happens in *research reactors*.

(2) Bombarding heavy nuclei with high energetic protons; the nuclei are "heated up" when a proton is absorbed and typically 20 - 30 neutrons are being evaporated. This process is called ***spallation*** and requires a *spallation source* with a proton accelerator and a heavy metal target station.

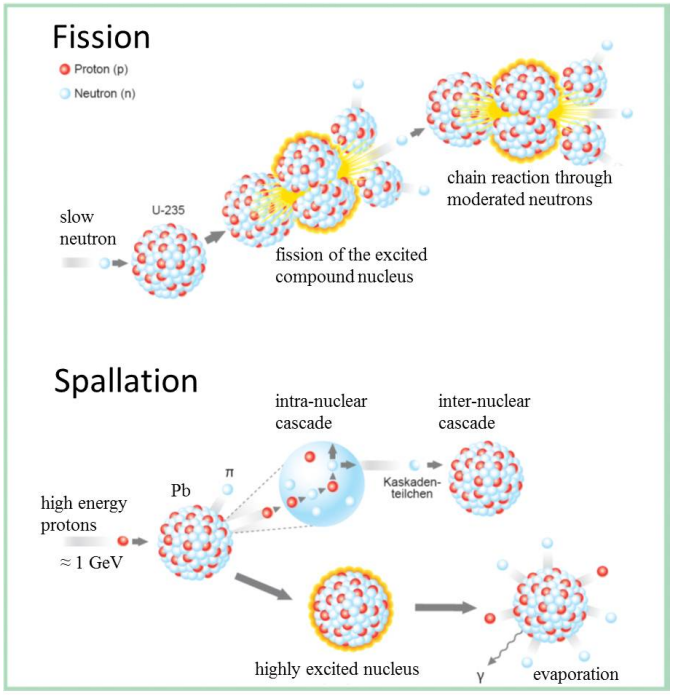

Fig. 8: *A cartoon of the processes of fission and spallation, respectively, used for the production of free neutrons (ess-reports).*

Both processes lead to free neutrons of energies in the MeV region. These neutrons are way too fast to be useful for condensed matter studies. These so-called epithermal neutrons have to be slowed down, which is done most efficiently by collisions with light atoms - e.g. Hydrogen H or Deuterium D in light or heavy water moderators, or C in graphite as in the first reactor, the Chicago Pile 1. During the moderation process after several collisions, the neutrons thermalize and acquire the temperature of the moderator. To adjust the energy spectra to ones need, mainly three types of moderators are being employed:

Moderator	Typical temperature [k]	Neutron energy range [meV]	Neutron wavelength range [Å]
hot source (graphite block)	2500	100 - 1000	0.3 - 0.9
thermal source (H_2O / D_2O)	300	5 - 100	0.9 - 4
cold source (liquid D_2)	25	0.05 - 5	4 - 40

Note that room temperature ~ 300 K corresponds an energy of about 26 meV (1 meV $\hat{=}$ 11.6 K), which is just a typical energy of elementary excitations in a solid. Despite the effort made in these high-tech facilities, the free neutrons available for scattering studies are still extremely rare. In a high flux reactor the neutron flux i. e. the number of neutrons passing through a given area in a given time is in the order of 10^{15} neutrons/cm^2·s. If one compares this value with particle fluxes in gases, the neutron density in high flux sources corresponds to high vacuum conditions of about 10^{-6} mbar pressure. The neutrons have to be transported from the source to the experimental areas, which can either be done by simple flight tubes or so called neutron guides. These are evacuated tubes with glass walls (often covered with metal layers to increase the performance), where neutrons are transported by total reflection from the side, top, and bottom walls in a similar manner like light in glass fibers. The neutron flux downstream at the scattering experiments is then even much lower than in the source itself and amounts to typically 10^6 - 10^8 neutrons/cm^2·s. This means that long counting times have to be taken into account to achieve reasonable statistics in the neutron detector. Just for comparison: the flux of photons of a small Helium-Neon laser with a power of 1 mW (typical for a laser pointer) amounts to some 10^{15} photons/s in a beam area well below 1 mm^2. At modern synchrotron radiation sources, a flux of some 10^{13} photon/s in a similar beamspot can be achieved.

Just as for synchrotron radiation with the XFEL, there is an European project to build the world's most powerful neutron source: the *European Spallation Source ESS*. It will outperform most existing sources by several orders of magnitude in peak flux and allow entirely new experiments to be realized [14]. A presentation of this project will be given by the acting CEO, Colin Carlile, as lecture C9.

3.3 Interaction Processes

The principle probes for condensed matter studies, X-rays, electrons and neutrons feature different interaction processes with matter, leading to a great complementarity. The principle interaction processes are depicted schematically in fig. 9. Details will be given in lecture A4.

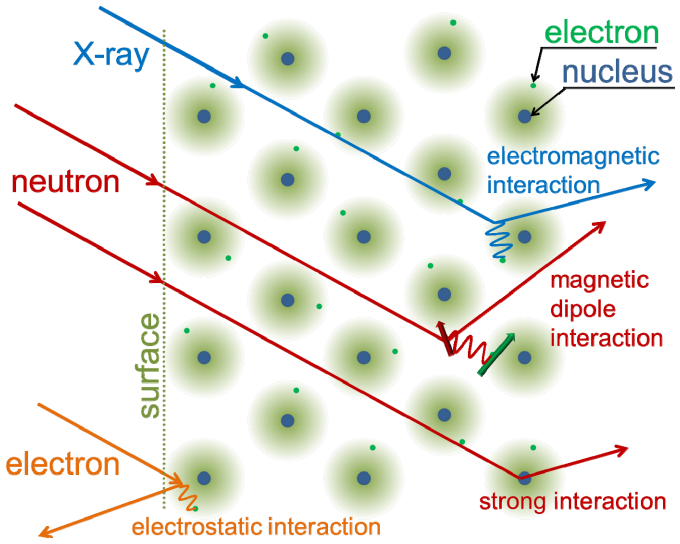

Fig. 9: *Cartoon of the scattering processes of X-rays, neutrons and electrons with atoms in a solid in a 2d representation. The most relevant interaction processes which lead to scattering events are indicated. Note that electrons are mainly scattered in a surface-near region.*

For X-rays, the most relevant scattering process is pure charge or *Thomson scattering* with the differential cross section for scattering from one electron of:

$$\frac{d\sigma}{d\Omega} = r_0^2 \cdot P(\theta) \qquad (21)$$

where $r_0 = \frac{e}{m_0 c^2} = 2.82\ fm$ is the classical electron radius and P(θ) a factor describing the polarization dependence of Hertz' dipole radiation. The Thomson scattering process is the basis for all structural investigations with X-rays since the discovery by Max von Laue one hundred years ago. A single electron is a point-like scatterer, leading to a cross section which is independent of Q, apart from the polarization dependence, Scattering from the extended electron cloud of an atom, on the other hand, leads to a variation of the scattered amplitude with scattering angle described by the so-called *formfactor* - the (normalized) Fourier transform of the electron density of a single atom.

Of course, X-rays as electromagnetic radiation also interact with the spin moment of the electron. This so-called *magnetic x-ray scattering* process is a relativistic correction to charge scattering and typically six orders of magnitude weaker. At absorption edges of elements, the scattering amplitude becomes energy dependent, leading to so-called *anomalous scattering*. Anomalous scattering (see figure 10) enables contrast variation, can also be used to enhance small scattering contributions, such as scattering from charge, orbital or magnetic order, see lecture D11. For most such studies, polarization handling is required, see lecture C7.

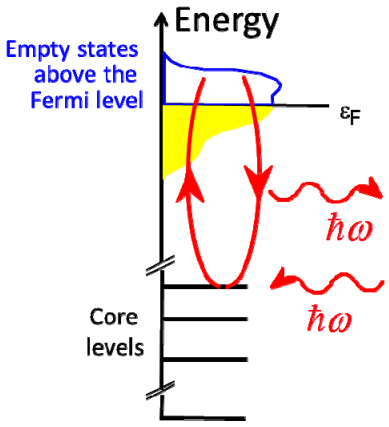

Fig. 10: *Schematic illustration of the second order perturbation process leading to anomalous scattering: core level electros are virtually excited by the incident X-rays into empty states above the Fermi level, if the photon energy is close to an absorption edge. Besides photoelectric absorption, a resonant scattering process can occur, where X-rays of the same wavelength are re-emitted.*

For neutron scattering, two main interaction processes are relevant: scattering with the nucleus due to the strong interaction (*nuclear scattering*) and scattering due to magnetic dipole-dipole interaction between the neutrons magnetic moment and the spin- or orbital moment of unpaired electrons in the solid (*magnetic scattering*).

Since the nucleus is a point-like object compared to the wavelength of thermal neutrons, the differential cross section for nuclear scattering is independent of scattering angle and given by:

$$\frac{d\sigma}{d\Omega} = |b|^2 \tag{22}$$

where b, the scattering length, is a phenomenological parameter as measure of the strength of the interaction potential. b depends not only on the atomic number, but also on the isotope and the nuclear spin orientation relative to the neutron spin.

Magnetic neutron scattering strongly depends on the polarization state of the neutron (for polarization handling, see lecture C6). The differential cross section is given by:

$$\frac{d\sigma}{d\Omega} = \left(\gamma_n r_0\right)^2 \left| -\frac{1}{2\mu_B} \langle \sigma_z' | \underline{\sigma} \cdot \underline{M}_\perp(\underline{Q}) | \sigma_z \rangle \right|^2 \tag{23}$$

The pre-factor $\gamma_n r_0$ has the value $\gamma_n r_0 = 0.539 \cdot 10^{-12}\ cm = 5.39\ fm$. $\underline{\sigma}$ denotes the spin operator, σ_z and σ_z' the polarization state of the neutron before and after the scattering process, respectively. $\underline{M}_\perp(\underline{Q})$ denotes the component of the Fourier transform of the sample magnetization, which is perpendicular to the scattering vector $\underline{Q}$:

$$\underline{M}_{\perp}(\underline{Q}) = \hat{\underline{Q}} \times \underline{M}(\underline{Q}) \times \hat{\underline{Q}}$$
$$\underline{M}(\underline{Q}) = \int \underline{M}(\underline{r}) e^{i\underline{Q}\cdot\underline{r}} d^3 r \qquad (24)$$

This tells us that with neutron scattering we are able to determine the magnetization $\underline{M}(\underline{r})$ in microscopic atomic spatial co-ordinates $\underline{r}$, which allows one not only to determine magnetic structures, but also the magnetization distribution within a single atom.

To obtain an idea of the size of the magnetic scattering contribution relative to nuclear scattering, we can replace the matrix element in (2.3) for a spin ½ particle by the value of one Bohr magneton 1 μ_B. This gives an "equivalent" scattering length for a magnetic scattering of 2.696 fm for a spin ½ particle. This value corresponds quite well to the scattering length of cobalt b_{co} = 2.49 fm, which means that magnetic scattering is comparable in magnitude to nuclear scattering.

3.4 Comparison of Probes

Figure 11 shows a double logarithmic plot of the dispersion relation "wave length versus energy" for the three probes neutrons, electrons and photons. The plot demonstrates, how thermal neutrons of energy 25 meV are ideally suited to determine interatomic distances in the order of 0.1 nm, while the energy of X-rays or electrons for this wavelength is much higher. However, with modern techniques at a synchrotron radiation source, energy resolutions in the meV-region become accessible even for photons of around 10 keV corresponding to a relative energy resolution $\Delta E/E \approx 10^{-7}$ (compare lectures D4, D8 and D9)! The graph also shows that colloids with a typical size of 100 nm are well suited for the investigation with light of energy around 2 eV. These length scales can, however, also be reached with thermal neutron scattering in the small angle region (compare lecture D1). While figure 11 thus demonstrates for which energy-wave-length combination a certain probe is particularly useful, modern experimental techniques extend the range of application by several orders of magnitude.

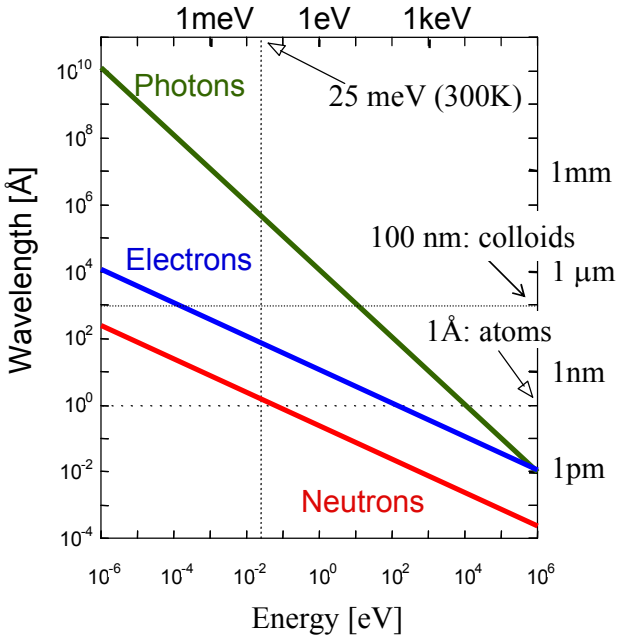

Fig. 11: *Comparison of the three probes - neutrons, electrons and photons - in a double logarithmic energy-wavelength diagram.*

It is therefore useful to compare the scattering cross sections as it is done in figure 12 for X-rays and neutrons. Note that the X-ray scattering cross sections are significantly larger as compared to the neutron scattering cross sections. This means that the signal for x-ray scattering is stronger for the same incident flux and sample size, but that caution has to be applied that the conditions for kinematical scattering are fulfilled. For X-rays, the cross section depends on the number of electrons and thus varies in a monotonic fashion throughout the periodic table. Clearly it will be difficult to determine hydrogen positions with x-rays in the presence of heavy elements such as metal ions. Moreover, there is a very weak contrast between neighbouring elements as can be seen from the transition metals Mn, Fe and Ni in figure 12. However, this contrast can be enhanced by anomalous scattering, if the photon energy is tuned close to the absorption edge of an element (lecture D11). Moreover, anomalous scattering is sensitive to the anisotropy of the local environment of an atom. For neutrons the cross sections depend on the details of the nuclear structure and thus vary in a non-systematic fashion throughout the periodic table. As an example, there is a very high contrast between Mn and Fe. With neutrons, the hydrogen atom is clearly visible even in the presence of such heavy elements as uranium. Moreover there is a strong contrast between the two hydrogen isotopes H and D. This fact can be exploited for soft condensed matter investigations by selectively deuterating certain molecules or functional groups and thus varying the contrast within the sample (see lectures E2, E3).

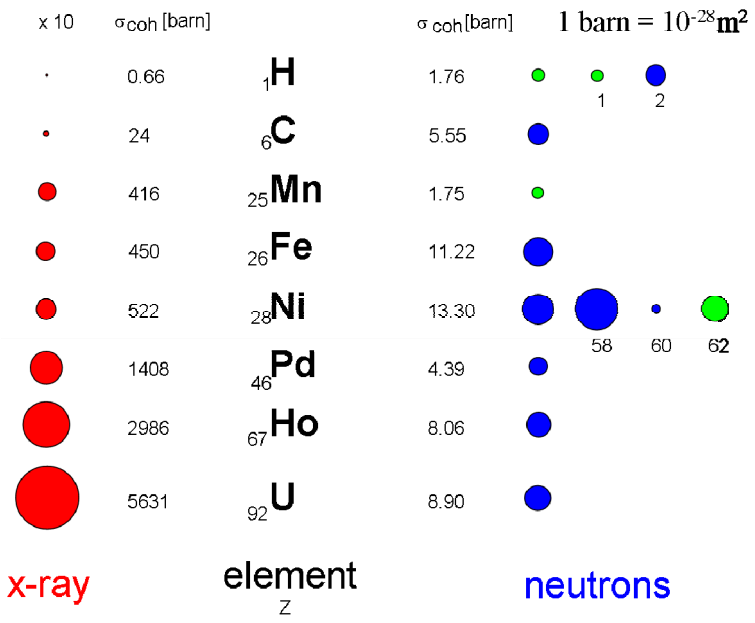

Fig. 12: *Comparison of the coherent scattering cross-sections for x-rays and neutrons for a selection of elements. The area of the coloured circles represent the scattering cross section. In the case of X-rays these areas were scaled down by a factor of 10. For neutrons, the green and blue coloured circles distinguish the cases where the scattering occurs with or without a phase shift of π.*

Finally, both neutrons and X-rays allow the investigation of magnetism on an atomic scale. Magnetic neutron scattering (lectures D3, D4, C6, …) is comparable in strength to nuclear scattering, while non-resonant magnetic X-ray scattering is smaller than charge scattering by several orders of magnitude. Despite the small cross sections, non-resonant magnetic x-ray Bragg scattering from good quality single crystals yields good intensities with the brilliant beams at modern synchrotron radiation sources. While neutrons are scattered from the magnetic induction within the sample, X-rays are scattered differently from spin and orbital momentum and thus allow one to measure both form factors separately. Inelastic magnetic scattering e.g. from magnons or so called quasielastic magnetic scattering from fluctuations in disordered magnetic systems is a clear domain of neutron scattering (lecture D4, D6). Finally, *resonance exchange scattering* XRES, a variant of anomalous X-ray scattering for magnetic systems, allows one not only to get enhanced intensities, but also to study magnetism with element- and band sensitivity (lecture D11).

With appropriate scattering methods, employing neutrons, X-rays or light, processes in condensed matter on very different time and space scales can be investigated. Which scattering method is appropriate for which region within the "scattering vector Q - energy E plane" is plotted schematically in figure 13. Via the Fourier transform, the magnitude of a scattering vector Q corresponds to a certain length scale, an energy to a certain frequency, so that the characteristic lengths and times scales for the various methods can be directly determined from the figure.

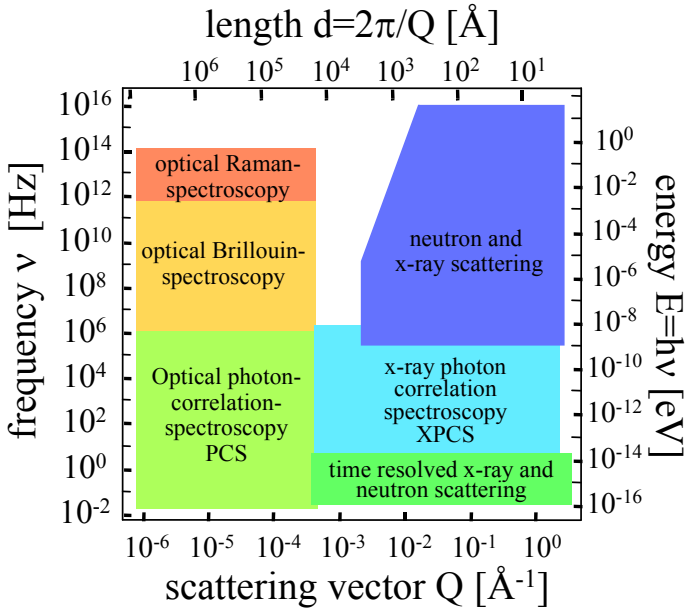

Fig. 13: *Regions in frequency ν and scattering vector Q (ν,Q)- or energy E and length d (E,d)-plane, which can be covered by various scattering methods.*

4 Techniques and Applications

4.1 Introduction

Scattering with electromagnetic radiation (light, soft- and hard-X-rays) and neutrons cover a huge range of energy and momentum transfers (see figure 13), corresponding to an extraordinary range of length- and time scales relevant for research in condensed matter. Exemplary, this is depicted for research with neutrons in figure 14.

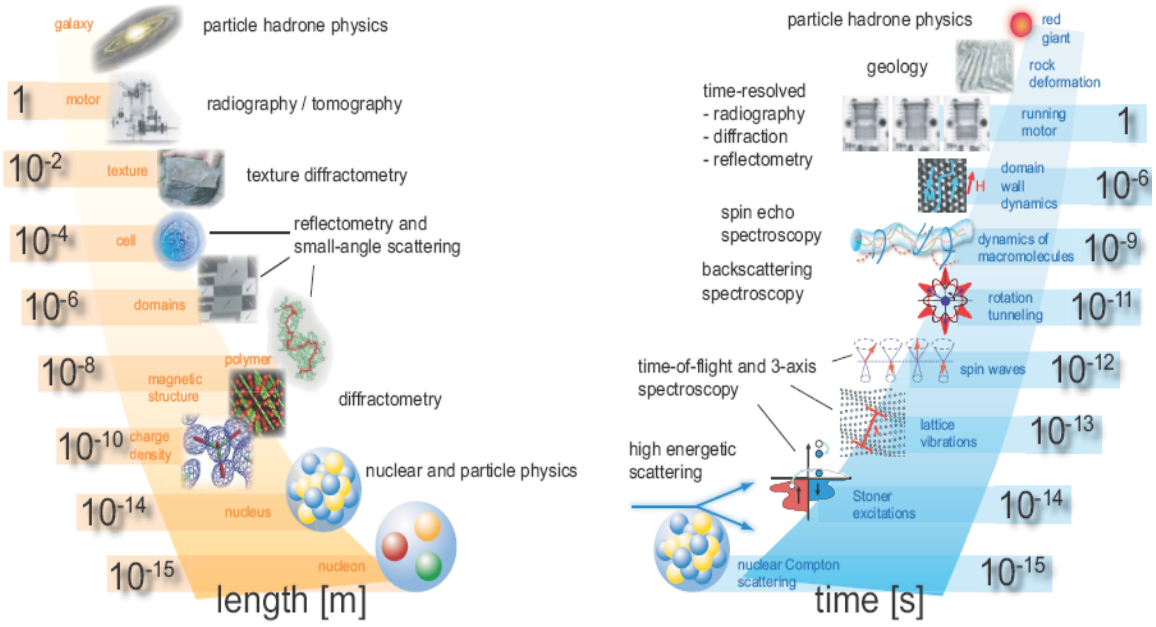

Fig. 14: *Length- and time scales covered by research with neutrons giving examples for applications and neutron techniques.*

The very extremes of length scales - below 10^{-12} m - are the domain of nuclear and particle physics, where e. g. measurements of the charge or the electric dipole moment of the neutron provide stringent tests of the standard model of particle physics without the need of huge and costly accelerators. On the other extreme, neutrons also provide information on length- and time scales relevant for astronomical dimensions, e. g. the decay series of radioactive isotopes produced by neutron bombardment give information on the creation of elements in the early universe. In this course, however, we are only concerned with neutrons as a probe for condensed matter research and therefore restrict ourselves to a discussion of neutron scattering. Still, the various scattering techniques cover an area in phase space from picometers pm up to meters and femtoseconds fs up to hours, a range, which probably no other probe can cover to such an extend.

Different specialized scattering techniques are required to obtain structural information on different length scales:

- With *wide angle diffractometry*, charge (X-rays) or magnetization (neutrons) densities can be determined within single atoms on a length scale of ca. 10 pm[2]. The position of atoms can be determined on a similar length scale, while distances between atoms lie in the 0.1 nm range (lectures B1, D3, D5, D11, E10).
- The sizes of large macromolecules, magnetic domains or biological cells lie in the range of nm to µm or even mm. For such studies of large scale structures, one applies

[2] In this sense, X-rays and neutrons are not only nanometer nm, but even picometer pm probes!

reflectometry (lectures D2, E5) or *small angle scattering technique* (lectures B2, D1, E2) or *imaging* (lectures F1, F2).

- Most materials relevant for engineering or geo-science occur neither in form of single crystals, nor in form of fine powders. Instead they have a grainy structure, often with preferred orientation of the grains. This so called texture determines the macroscopic strength of the material along different directions. *Texture diffractometry* as a specialized technique allows one to determine this granular structure on length scales of up to mm (high energy X-ray diffraction as "3d microscope").
- Finally, for even larger structures, one uses imaging techniques, such as neutron *radiography* or *tomography* (lecture F2), which give a two dimensional projection or full 3-dimensional view into the interior of a sample due to the attenuation of the beam, the phase shift or other contrast mechanisms.

In a similar way, specialized scattering techniques are required to obtain information on the system's dynamics on different time scales:

- *Neutron Compton scattering*, where a high energy neutron in the eV energy range makes a deep inelastic collision with a nucleus in so-called impulse approximation, gives us the momentum distribution of the atoms within the solid. Interaction times are in the femtosecond fs time range.
- With *pump-probe techniques* at free electron lasers, processes in the fs to ps time range can be studied. For this technique one uses the time structure of the radiation and delays a "probe" pulse with respect to the "pump" pulse to study e.g. relaxation processes after excitation in real time.
- In magnetic metals, there exist single particle magnetic excitations, so-called Stoner excitations, which can be observed with inelastic scattering of high energy neutrons using the so-called *time-of-flight spectroscopy* or the *triple axis spectroscopy* technique (lecture D4). Typically, these processes range from fs to several hundred fs.
- The electronic structure of solids, including electronic relaxation processes in the fs time range, can be determined by X-ray spectroscopy techniques (lecture F3, F4).
- Lattice vibrations (phonons) or spin waves in magnetic systems (magnons) have frequencies corresponding to periods in the picosecond ps time range (lecture B4). Again these excitations can be observed with neutron *time-of-flight-*, neutron *triple axis spectroscopy* or at high energy resolution backscattering synchrotron beamlines (lecture D4).
- Slower processes in condensed matter are the tunneling of atoms, for example in molecular crystals or the slow dynamics of macromolecules (lectures B6, E3, E8). Characteristic time scales for these processes lie in the nanosecond ns time range. They can be observed with specialized techniques such as neutron *backscattering spectroscopy*, neutron *spin-echo spectroscopy*, light- or X-ray photon correlation spectroscopy (lecture D8).
- Even slower processes occur in condensed matter on an ever increasing range of lengths scales. One example is the growth of domains in magnetic systems, where domain walls are pinned by impurities. These processes may occur with typical time

constants of microseconds μs. Periodic processes on such time scales can be observed with *stroboscopic scattering* techniques.

- Finally, *time resolved scattering* or *imaging* techniques, where data is taken in consecutive time slots, allow one to observe processes from the millisecond ms to the hour h range.

Even within a spring school of two weeks, it is impossible to cover all scattering techniques and applications. Some will be touched briefly in the application lectures, but we have not foreseen specialized lectures e.g. for texture and strain analysis, or nuclear (neutrons) and electronic (X-rays) Compton scattering.

4.2 Correlation functions

This somewhat advanced section is intended for readers already familiar with scattering and can be skipped during first reading. It is given here for completeness. For details we refer to lecture A5. For sake of simplicity, formulas are given only for neutron scattering, but similar expressions hold for X-ray scattering.

The neutron scattering cross section for nuclear scattering can be expressed in the following form (for simplicity, we restrict ourselves to a mono-atomic system):

$$\frac{\partial^2\sigma}{\partial\Omega\partial\omega} = \frac{k'}{k}\cdot N\cdot\left[\left(\overline{|b|^2}-|\bar{b}|^2\right)S_{inc}(\underline{Q},\omega)+|\bar{b}|^2\ S_{coh}(\underline{Q},\omega)\right] \tag{25}$$

The cross section is proportional to the number N of atoms. It contains a kinematical factor k'/k, i. e. the magnitude of the final wave vector versus the magnitude of the incident wave vector, which results from the phase-space density. The scattering cross section contains two summands: one is the coherent scattering cross section, which depends on the magnitude square of the average scattering length density $|\bar{b}|^2$ and the other one is the incoherent scattering, which depends on the variance of the scattering length $\left(\overline{|b|^2}-|\bar{b}|^2\right)$. The cross section (25) has a very convenient form: it separates the interaction strength between probe (the neutrons) and sample from the properties of the system studied. The latter is given by the so-called scattering functions $S_{coh}(\underline{Q},\omega)$ and $S_{inc}(\underline{Q},\omega)$, which are completely independent of the probe and a pure property of the system under investigation. The *coherent scattering function* $S_{coh}(\underline{Q},\omega)$ (also called *dynamical structure factor* or *scattering law*) is a Fourier transform in space and time of the pair correlation function:

$$S_{coh}(\underline{Q},\omega) = \frac{1}{2\pi\hbar}\int G(\underline{r},t)e^{i(\underline{Q}\cdot\underline{r}-\omega t)}d^3rdt \tag{26}$$

Here the *pair correlation function* $G(\underline{r},t)$ depends on the time dependent positions of the atoms in the sample:

$$G(\underline{r},t) = \frac{1}{N}\sum_{ij}\int \left\langle \delta(\underline{r}' - \underline{\mathrm{r}}_{\mathrm{i}}(0)) \cdot \delta(\underline{r}' + \underline{r} - \underline{\mathrm{r}}_{\mathrm{j}}(t)) \right\rangle d^3 r' \\ = \frac{1}{N}\int \left\langle \rho(\underline{r}',0) \cdot \rho(\underline{r}' + \underline{r},t) \right\rangle d^3 r' \tag{27}$$

$\underline{r}_i(0)$ denotes the position of atom *i* at time *0*, while $\underline{r}_j(t)$ denotes the position of another atom *j* at time *t*. The angle brackets denote the thermodynamic ensemble average, the integral extends over the entire sample volume and the sum runs over all atom pairs in the sample. Instead of correlating the positions of two point-like scatterers at different times, one can rewrite the pair correlation function in terms of the particle density as given in the second line of (27). Coherent scattering arises from the superposition of the amplitudes of waves scattered from one particle at time *0* and a second particle at time *t*, averaged over the entire sample volume and the thermodynamic state of the sample. In contrast, incoherent scattering arises from the superposition of waves scattered from the same particle at different times. Therefore the *incoherent scattering function* $S_{inc}(\underline{Q},\omega)$ is given in the following form:

$$S_{inc}(\underline{Q},\omega) = \frac{1}{2\pi\hbar}\int G_s(\underline{r},t) e^{i(\underline{Q}\cdot\underline{r}-\omega t)} d^3 r dt \tag{28}$$

which is the Fourier transform in space and time of the *self correlation function* $G_S(\underline{r},t)$:

$$G_s(\underline{r},t) = \frac{1}{N}\sum_{j}\int \left\langle \delta(\underline{r}' - \underline{\mathrm{r}}_{\mathrm{j}}(0)) \cdot \delta(\underline{r}' + \underline{r} - \underline{\mathrm{r}}_{\mathrm{j}}(t)) \right\rangle d^3 r' \tag{29}$$

We next define the *intermediate scattering function* $S(\underline{Q},t)$ as the purely spatial Fourier transform of the correlation function (here we have dropped the index “coh” and “inc”, respectively, as the intermediate scattering function can be defined for coherent as well as for incoherent scattering in the same way):

$$S(\underline{Q},t) := \int G(\underline{r},t) e^{i\underline{Q}\cdot\underline{r}} d^3 r \\ = S(\underline{Q},\infty) + S'(\underline{Q},t) \tag{30}$$

For reasons, which will become apparent below, we have separated in the second line the intermediate scattering function for infinite time

$$S(\underline{Q},\infty) = \lim_{t\to\infty} S(\underline{Q},t) \tag{31}$$

from the time development at intermediate times. Given this form of the intermediate scattering function $S(\underline{Q},t)$, we can now calculate the scattering function as the temporal Fourier transform of the intermediate scattering function:

$$S(\underline{Q},\omega)=\frac{1}{2\pi\hbar}\int_{-\infty}^{+\infty}S(\underline{Q},t)e^{-i\omega t}dt \quad =\frac{1}{2\pi\hbar}\int_{-\infty}^{+\infty}\left[S(\underline{Q},\infty)+S'(\underline{Q},t)\right]e^{-i\omega t}dt$$
$$=\underbrace{\frac{1}{\hbar}\delta(\omega)S(\underline{Q},\infty)}_{elastic\ scattering}+\underbrace{\frac{1}{2\pi\hbar}\int_{-\infty}^{+\infty}S'(\underline{Q},t)e^{-i\omega t}dt}_{inelastic\ scattering} \tag{32}$$

In this way, the scattering function has been separated into one term for frequency *0*, i. e. vanishing energy transfer $\Delta E=\hbar\omega=0$ and one term for non-vanishing energy transfer. The first term is the purely elastic scattering, which is given by the correlation function at infinite times. Correlation at infinite times is obtained for particles at rest. A prominent example is the Bragg scattering from a crystalline material, which is purely elastic, while the scattering from liquids is purely inelastic, since the atoms in liquids are moving around freely and thus the correlation function vanishes in the limit of infinite time differences.

Often times the energy of the scattered neutron is not discriminated in the detector. In such experiments, where the detector is set at a given scattering angle, but does not resolve the energies of the scattered neutrons, we measure an *integral cross section* for a fixed direction $\hat{\underline{k}}'$ *of* $\underline{k}'$:

$$\left(\frac{d\sigma}{d\Omega}\right)_{coh,\mathrm{int}}=\int\left.\frac{\partial^2\sigma}{\partial\Omega\partial\omega}\right|_{\hat{\underline{k}}'=const}\cdot d\omega \tag{33}$$

Momentum and energy conservation are expressed by the following kinematic equations of scattering:

$$\hbar\underline{Q}=\hbar\underline{k}'-\hbar\underline{k};\ \hbar\omega=E-E'=\frac{\hbar^2}{2m}\left(k^2-k'^2\right) \tag{34}$$

Due to these kinematic conditions, the scattering vector $\underline{Q}$ will vary with the energy of the scattered neutron E' or the energy transfer $\hbar\omega$ when the integral in (33) is performed. The so-called *quasi-static approximation* neglects this variation and uses the scattering vector $\underline{Q}_0$ for elastic scattering $(\hbar\omega=0)$ in (33). This approximation is valid only if the energy transfer is small compared to the initial energy. This means that the movements of the atoms are negligible during the propagation of the radiation wave front from one atom to the other. In this case, the above integral can be approximated as follows:

$$\left(\frac{d\sigma}{d\Omega}\right)_{coh,QSA}=\frac{k'}{k}\frac{N}{2\pi\hbar}\int\left(\int G(\underline{r},t)e^{i(\underline{Q}_0\cdot\underline{r}-\omega\cdot t)}d^3rdt\right)d\omega$$
$$=\frac{k'}{k}\frac{N}{2\pi\hbar}\int G(\underline{r},t)e^{i\underline{Q}_0\cdot\underline{r}}\delta(t)d^3rdt=\frac{k'}{k}\frac{N}{2\pi\hbar}\int G(\underline{r},0)e^{i\underline{Q}_0\cdot\underline{r}}d^3r \tag{35}$$

which shows that the integral scattering in quasi-static approximation depends on the *instantaneous spatial correlation function* only, i. e. it measures a snapshot of the arrangement of atoms within the sample. This technique is e. g. very important for the determination of short-range order in liquids, where no elastic scattering occurs (see above).

Our discussion on correlation functions can be summarized in a schematic diagrammatic form, see figure 15.

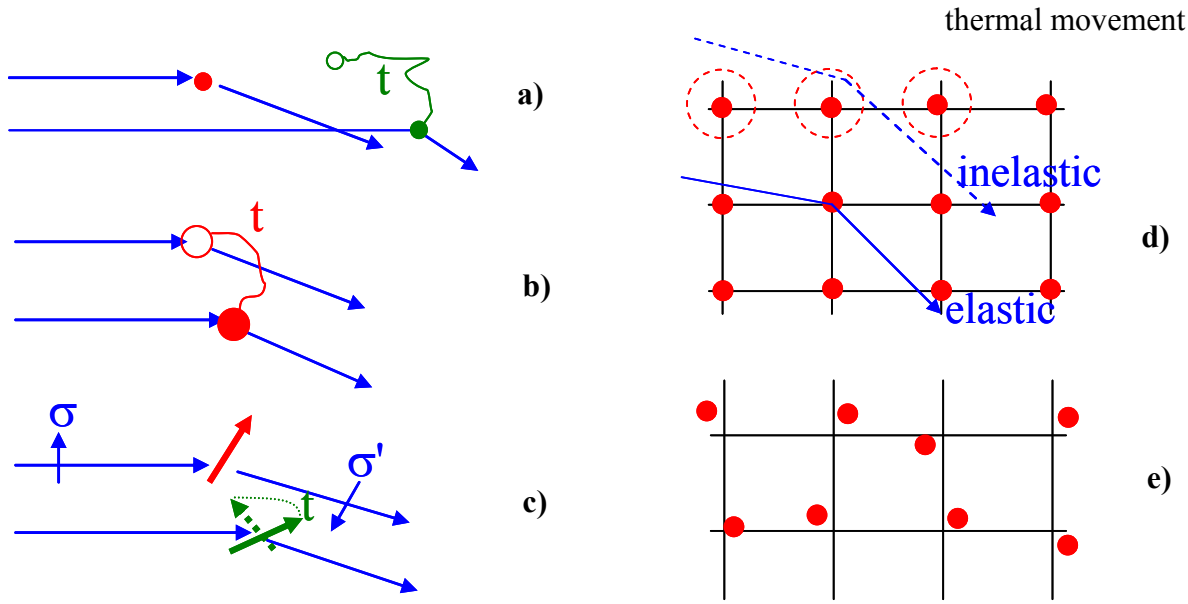

Fig. 15: *Schematic diagrams depicting the various scattering processes: a) coherent scattering is connected with the pair correlation function in space-and time; b) incoherent scattering is connected with the self-correlation function; c) magnetic scattering is connected with the spin pair correlation function; d) elastic and inelastic scattering from a crystal measures average positions and movements of the atoms, respectively, e) inelastic scattering in quasistatic approximation sees a snapshot of the sample.*

Figure 15 shows that coherent scattering is related to the pair correlation between different atoms at different times (15a), while incoherent scattering relates to the one particle self correlation function at different times (15b). In analogy to nuclear scattering, magnetic scattering depends on the correlation function between magnetic moments of the atoms. If the magnetic moment is due to spin only, it measures the *spin pair correlation function* (15c). Since the magnetic moment is a vector quantity, this correlation function strongly depends on the neutron polarization. For this reason, in magnetic scattering we often perform a polarization analysis as discussed in the corresponding lecture C6. Figure 15d depicts elastic and inelastic scattering from atoms on a regular lattice. Elastic scattering depends on the infinite time correlation and thus gives us information on the time averaged structure. Excursions of the atoms from their time averaged positions due to the thermal movement will give rise to inelastic scattering, which allows one e. g. to determine the spectrum of lattice vibrations, see lecture D4 on “inelastic scattering”. Finally, an experiment without energy analysis in quasistatic approximation will give us the instantaneous correlations between the atoms, see figure 15e. This schematic picture shows a snapshot of the atoms on a regular lattice. Their positions differ from the time averaged positions due to thermal movement.

It is evident that specialized techniques are needed to obtain all the information contained in the various cross sections. Optical elements needed to define incident and final wave vectors, and detectors to count the scattered particles, will be discussed in lectures C3, C4, C5, C6 and C7. It is important, however, to realize that these optical elements are never perfect and thus in reality a distribution of initial and final wave vectors are being selected. Therefore, the measured intensity in the detector is not simply proportional to the scattering function $S(\underline{Q},\omega)$ (or more precisely, the cross section), but it is proportional to the convolution of the scattering function (or cross section) with the *experimental resolution function R*:

$$I(\underline{Q}_0,\omega_0) \propto \iint S(\underline{Q},\omega)R(\underline{Q}_0-\underline{Q},\omega_0-\omega)d^3Qd\omega \tag{36}$$

Here, the resolution function *R* appears due to the limited ability of any experimental setup to define an incident or final wave vector $\underline{k}$ or $\underline{k}'$, respectively. *R* therefore depends purely on the instrumental parameters and not on the scattering system under investigation. The art of any scattering experiment is to adjust the instrument - and with it the resolution function - to the problem under investigation. If the resolution of the instrument is too tight, the intensity in the detector becomes too small and counting statistics will limit the precision of the measurement. If, however, the resolution is too relaxed, the intensity will be smeared out and will not allow one to determine the scattering function properly.

4.3 Selected examples for applications

Here we give some selected examples for applications of scattering experiments to topical research, which we selected mainly from our own research at Forschungszentrum Jülich.

4.3.1 Diffractometry

Let us start with structure determination on various length scales. The scattering cross section is related to the Fourier transform of the spatial correlation function and therefore a reciprocal relation exists between characteristic real space distances *d* and the magnitude of the scattering vector *Q*, for which intensity maxima appear:

$$\Delta Q \sim \frac{2\pi}{d} \tag{37}$$

Bragg scattering from crystals provides an example for this equation: the distance between maxima of the Laue function is determined by $\Delta Q \cdot d = 2\pi$, where *d* is the corresponding real space periodicity. (37) is central for the choice of an instrument or experimental set-up, since it tells us which Q-range we have to cover in order to get information on a certain length range in real space.

In order to calculate the corresponding scattering angle, we make use of (3) to calculate 2θ, the scattering angle $\sphericalangle(\underline{k},\underline{k}')$. This angle has to be large enough in order to separate the scattering event clearly from the primary beam. This is why we need different instruments to study materials on different length scales. Table 1 gives two examples.

Example	d	ΔQ	2θ (λ=1 Å)	2θ (λ=10 Å)	Technique
Distance between atoms in crystals	2 Å	3.14 $Å^{-1}$	29°	"cut-off"	wide angle diffraction
Precipitates in metals (e.g. Co in Cu)	400 Å	0.016$Å^{-1}$	0.14°	1.46°	small angle scattering

Tab. 1: *Examples for scattering from structures on different characteristic real space length scales d. ΔQ is the corresponding characteristic scattering vector according to (37), 2θ the scattering angle according to (3), calculated for two different wavelength λ.*

1. The study of structures on atomic length scales is typically done with a wavelength of around 1 Å (comparable to the distance between the atoms) and the scattered intensity is observed at rather large angles between 5° and 175°. Therefore one speaks of *wide angle diffraction*, which is employed for the study of atomic structures.
2. For the study of large scale structures (precipitates, magnetic domains, macromolecules in solution or melt) on length scales of 10 up to 10,000 Å (1 up to 1000 nm), the magnitude of the relevant scattering vectors as well as the corresponding scattering angles are small. Therefore one chooses a longer wavelength in order to expand the diffractogram. The suitable technique is *small angle scattering*, which is employed to study large scale structures.

A topical example for wide angle diffraction comes from the field of superconductivity (lecture E1), which celebrated the 100 anniversary of its discovery just last year, see figure 16.

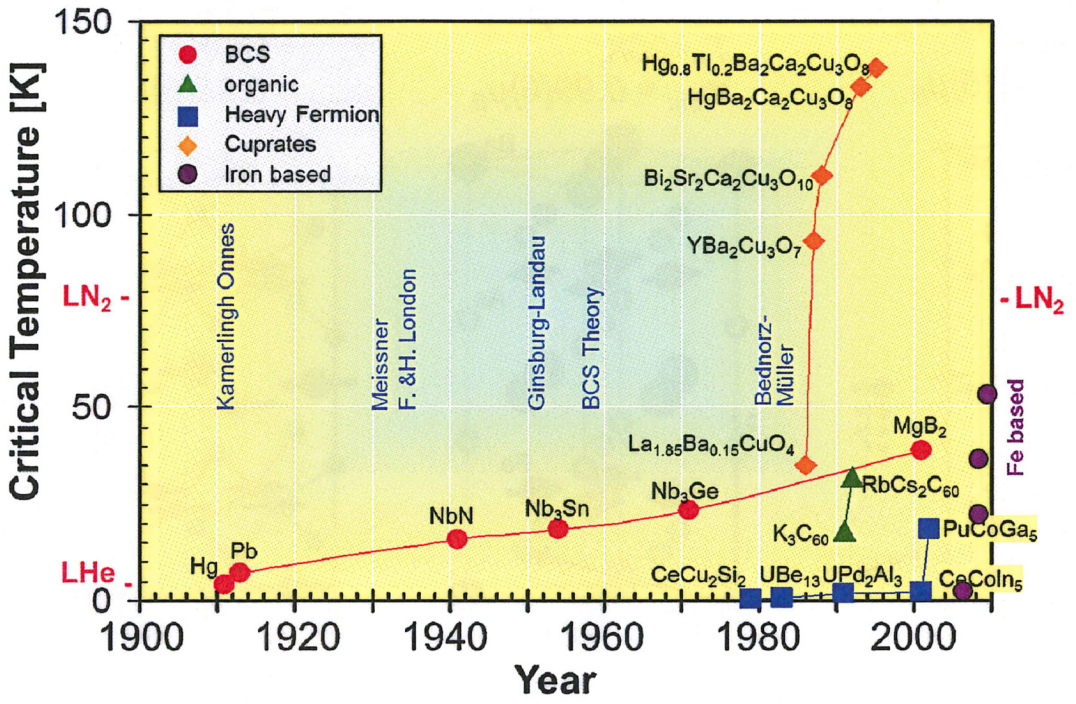

Fig. 16: *A brief history of superconductivity with some examples of superconducting compounds. The critical temperature for the onset of superconductivity T_c is plotted versus the year of discovery.*

The mechanism of superconductivity for the so-called BCS (Bardeen, Cooper, Schrieffer), superconductors is well understood as a Bose-Einstein condensation of Cooper pairs, i.e. electrons bound by the exchange of phonons. More than 25 years ago, Bednorz and Müller (Nobel prize in physics 1987) discovered a new family of superconductors with transition temperatures exceeding liquid nitrogen temperatures, the cuprate superconductors. Despite huge efforts of solid state scientists world wide, the mechanism of superconductivity in these compounds is still unresolved. Therefore it came as a big relieve, when a few years ago a new class of high temperature superconductors was discovered, which is iron based. Just like for cuprates, these superconductors show an intimate proximity to magnetism, i.e. the parent compounds show magnetic order. X-ray and neutron diffraction was employed to determine the structure and magnetic structure of these compounds ([15 - 19]), see figure 17.

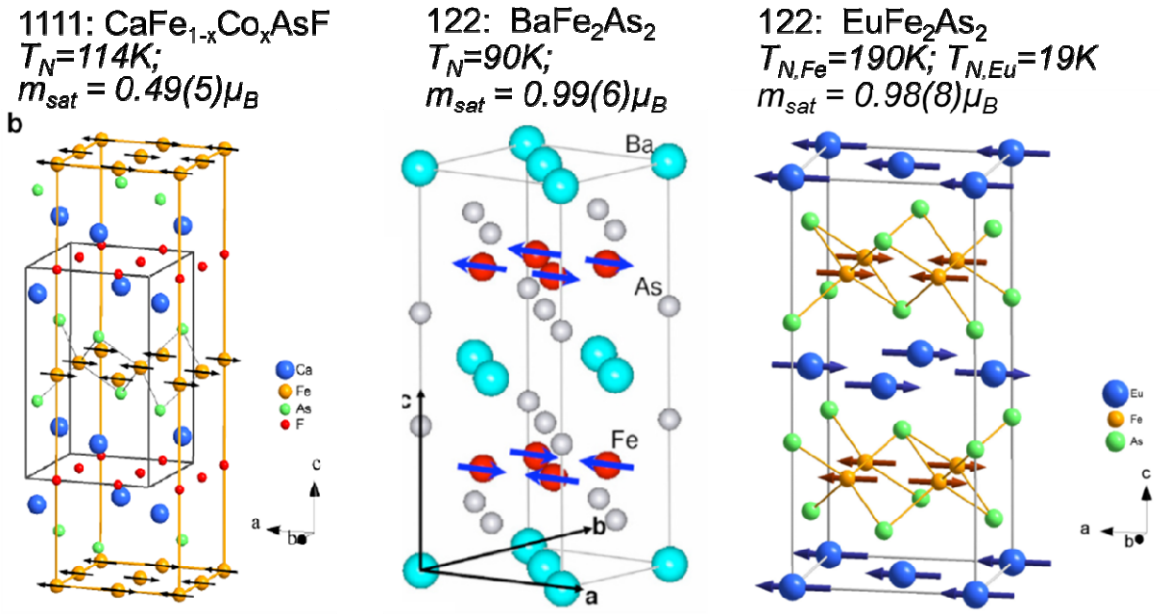

Fig. 17: *Magnetic structures of some iron based superconductors determined by wide angle diffraction .*

This structural information is an essential prerequisite for an understanding of superconductivity in these compounds. All iron-arsenide superconductors have in common that they are layered structures with Fe tetrahedrally surrounded by As. In fact, the closer the bond angles to a perfect tetrahedron, the higher the transition temperature. The magnetic structure is stripe-like with a rather small moment, indicating frustration and/or spin density wave mechanisms.

Wide angle scattering can provide even much more detailed information, such as the magnetization density distribution within the unit cell [20] (for this study, polarized neutrons are required), or the phase diagram as function of temperature, field or pressure [21].

A topical example for small angle scattering stems from the study of magnetic nanoparticles [22]. Magnetic nanoparticles are of fundamental interest for the understanding of magnetism on the nanoscale. They have potential for applications as ferrofluids, in medicine and magnetic data storage. The internal structure of such particles can be determined with a special wide angle scattering technique, the *Pair Distribution Function* PDF analysis (lecture D5). With polarized small angle neutron scattering, the magnetic structure of such particles can be determined, where one finds a significant reduction of the magnetic moment as compared to its bulk value and a spin canting in a surface near layer of the particle [23]. Of special interest is the self assembly of such nanoparticles into 2-dimensional or 3-dimensional ordered structures. We were able to grow well-ordered mesocrystals of maghemite nanoparticles on a silicon wafer substrate. In order to analyse the depth resolved mesocrystal

structure, small angle x-ray scattering is performed under grazing incidence of the beam at a synchrotron radiation facility. Figure 18 shows an example of such a measurement.

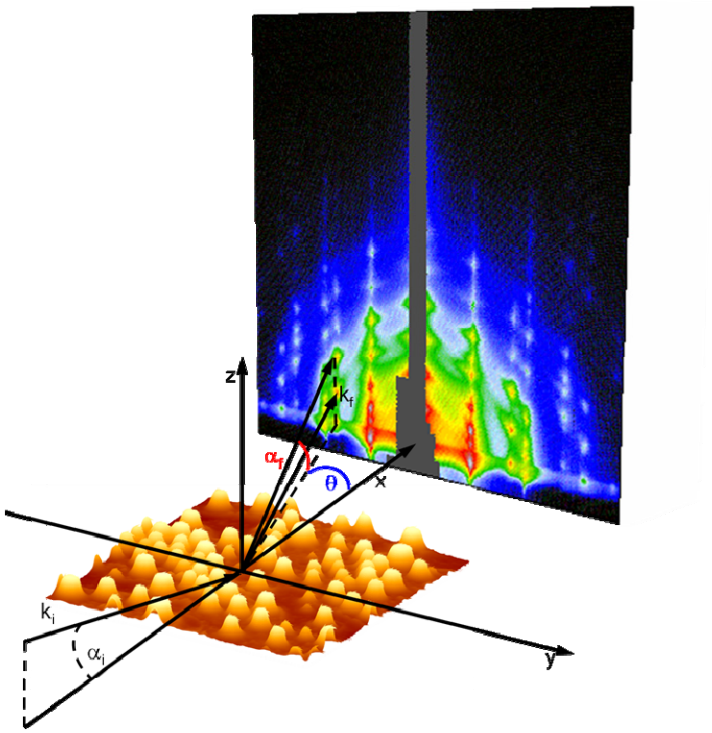

Fig. 18: *Scheme showing the principle of Grazing Incidence Small Angle X-ray Scattering GISAXS with an actual diffraction pattern from mesocrystals of magnetic nanoparticles .*

It turns out that quite complex structures develop. As an example, figure 19 shows the structure obtained for truncated maghemite cubes with 8.5 nm edge length. The body centred tetragonal structure found had been predicted to exist, but had never been observed before.

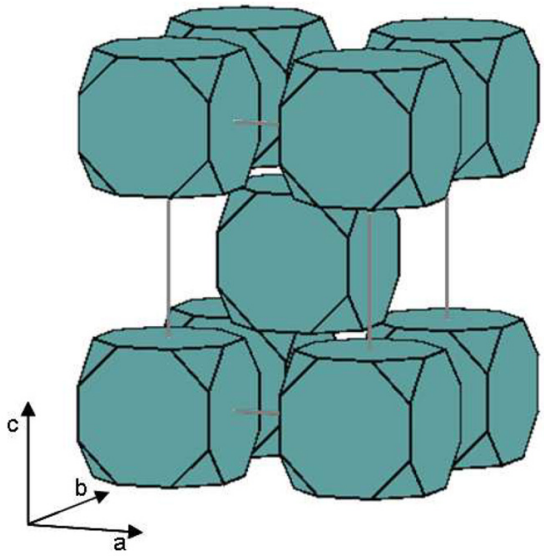

Fig. 19: *Schematic diagram of the body centered tetragonal structure found for truncated nanocubes of maghemite [24].*

From a systematic series of such studies, the interaction energies can be determined. The ability to modulate interparticle interactions by a variation of the particle shape is promising to open a new direction in crystallography, where the mesocrystal structure depends largely on the shape of the primary constituents [24].

4.3.2 Spectroscopy

While diffraction provides information on "where the atoms are", spectroscopy tells us "how the atoms move". Again, this is a very wide field, from diffusion of single atoms or molecules (lecture B3), via coherent elementary excitations in solids (lattice vibrations, spin waves, see lecture B4) and local excitations such as crystal field transitions (lecture B5) to the dynamics of large molecules (lecture B6) like polymers (lecture E3), proteins (lecture E8) or glasses (lecture E9). Just like for diffraction, we can only give two representative examples.

The first example is again concerned with the iron based superconductors. If we want to answer the question, whether the coupling of electrons to Cooper pairs is mediated through phonons, we have to know the phonon dispersion and/or look at charges in the phonon density of states between the superconducting and non-superconducting states. The phonon dispersion is best determined by neutron triple axis or inelastic x-ray spectroscopy (lecture D4). Phonon density of states are measured via time-of-flight neutron scattering (total phonon density of states) or nuclear resonant x-ray scattering (element specific, lecture D9). As an example, figure 20 shows the phonon dispersion of one of the parent compounds of the Fe-As superconductors [25].

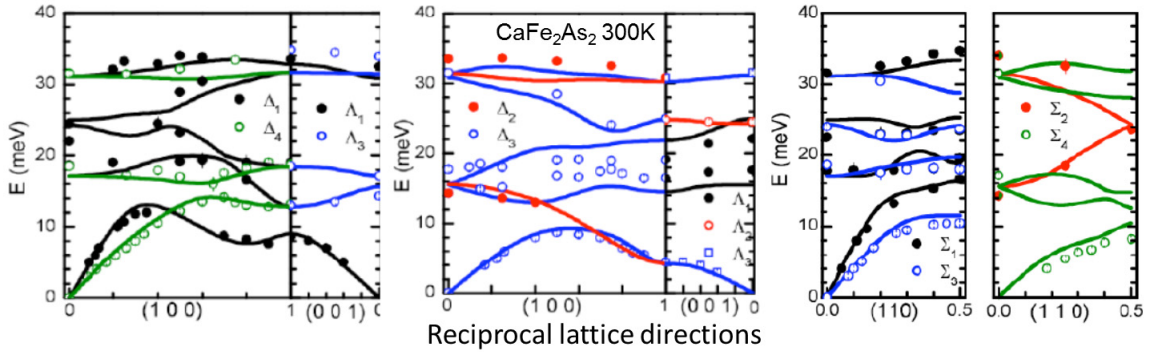

Fig. 20: *Phonon dispersion of $CaFe_2As_2$ at room temperature along main symmetry directions. Data from neutron triple axis spectroscopy are compared to ab-initio calculations (solid lines) [25].*

The calculations largely reproduce the measurements with the exception of some branches, where calculated energies deviate or a strong damping of modes containing only Fe atoms is observed. Similar studies can be performed under applied pressure. Due to the small sample volume, inelastic x-ray scattering is ideally suited to study pressure dependence of phonon modes [26]. Systematic studies of the phonon density of states have been done as well for the non-superconducting as for the superconducting phases [27-30]. At this stage, it is commonly agreed that coupling of electrons to Cooper pairs through phonons alone is not likely to be the mechanism leading to superconductivity in these iron based superconductors. In fact, magnetism has to be involved to reproduce the phonon spectra. Magnetic fluctuations have been observed in the non-superconducting and the superconducting phases and a coupling scheme through magnetic fluctuations, possibly combined with lattice vibrations, is currently being considered.

This example shows clearly, how scattering methods can access microscopic information, which directly relates to the mechanism leading to a macroscopic quantum phenomenon such as superconductivity (see also lecture E1). A similar example can be given from the field of life science for high resolution spectroscopy. Large biomolecules show a slow dynamics in the nsec time range, which requires techniques such as neutron spin echo or photon correlation spectroscopy.

Proteins are the molecular machinery of life. As nanomachines of metabolism, they are in every cell of our body tirelessly active to transport, synthesize, divide and transform substances. The ability of specific proteins to do their job is determined by the sequence of amino acids and their three-dimensional arrangement as determined by x-ray protein crystallography (lecture E10), but also depends on structural rearrangements. To perform their function structural changes are often important. They reach from atomic reorientation to rearrangements of complete domains to enclose substrates, to release products or to reconfigure domains in complexes. Neutron Spin Echo Spectroscopy is a versatile tool to

investigate these large scale movements in biomolecules on different length scales with the ability to determine the timescale of the motions.

The protein alcohol dehydrogenase (ADH) is responsible for the interconversion between alcohol and ketons - a very important catalysis reaction for detoxification after alcohol abuse, see figure 21.

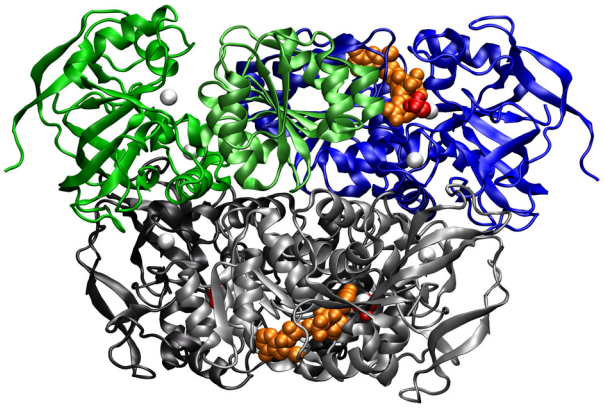

Fig. 21: *The protein alcohol dehydrogenase. The exterior (catalytic) domain tilts outwards and opens the cleft which initiates the catalytic reaction.*

With neutron spin echo spectroscopy, the internal dynamics of the molecule could be studied and the motional amplitude of 0.8 nm determined - an important step in understanding the functionality of proteins in catalytic reactions [31], see lecture E8.

These few selected examples serve to give a taste of the capabilities of scattering methods. More examples will be given in the lectures on topical applications E1 - E9.

With the planned European facilities ESS and XFEL, the future of scattering methods is extremely bright. The high intensity and brightness of these sources will enable entirely new experiments. With neutron chopper spectrometers at ESS, dispersion relations of elementary excitations can be mapped within a few minutes, allowing parametric spectroscopic studies as function of field, pressure or temperature as they are done today for structural studies on diffractometers. Fully coherent scattering of radiation from the XFEL permits the use of oversampling techniques and possibly the determination of the structure of biomolecules without the need for crystallization. The time structure of XFEL with the < 100 fs flashes will allow one to study time dependencies e.g. of chemical reactions in the corresponding time window. The two European projects ESS and XFEL and the possible new types of applications will be presented in lectures C8, C9 and D10.

5 Life at large scale facilities

Neutron and x-ray sources are rather expensive to build and to operate. Therefore, only few such installation exist world wide - especially in the field of research with neutrons, where licensing of nuclear installations is an additional aspect to be considered. Figure 22 shows the geographic distribution of the major facilities for research with neutrons. The Jülich Centre for Neutron Science JCNS is present at some of the world's best sources.

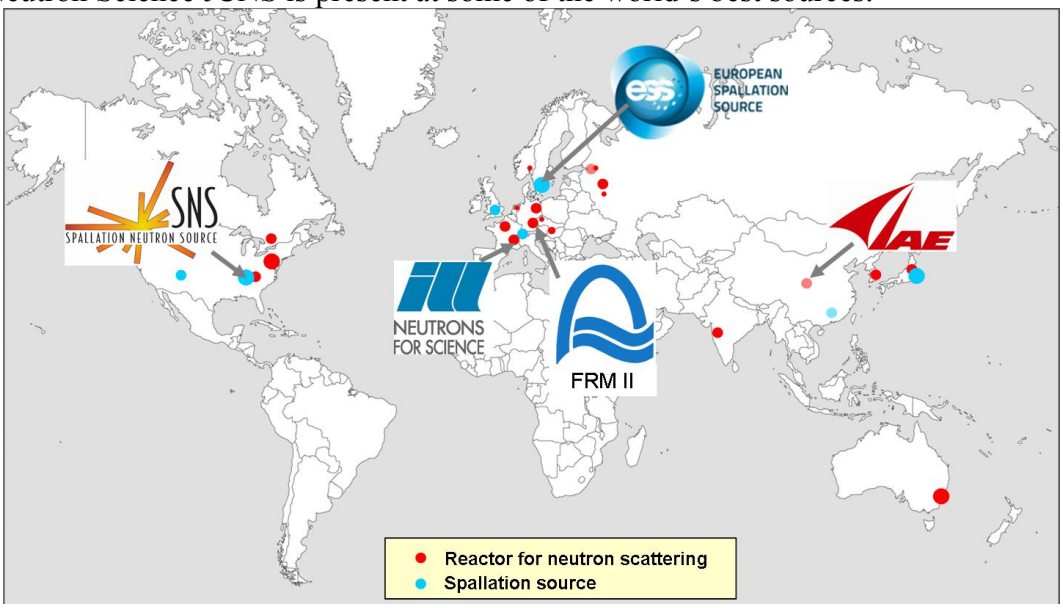

Fig. 22: *Major neutron research centres worldwide which have sources of appreciable flux and a broad instrumentation suite for condensed matter research. JCNS is present at four of the leading sources worldwide: the neutron research reactor FRM II in Garching, Germany, the Institute Laue-Langevin ILL in Grenoble, France, the Spallation Neutron Source SNS in Oak Ridge, USA and the Chinese Advanced Research Reactor CARR close to Beijing, China. JCNS also has a leading involvement in the European Spallation Source project, Lund, Sweden.*

The fact that there are only few sources worldwide implies that experiments at large facilities have to be organized quite different from normal lab-based experiments. Efforts have to be made to use the existing sources as efficient as possible. This means (i) continuous and reliable operation of the source during a large fraction of the year; (ii) many highly performing instruments, which can run in parallel, located around every source; (iii) professional instrument operation with highly qualified staff and a stringent risk management to keep the downtime of instruments and auxiliary equipment as low as possible; (iv) and access for as many scientists as possible. While there are specialized companies which produce beamline and instrument components, there is no true commercial market for neutron or synchrotron instruments. Therefore these instruments are being built by research centres, where usually one or a few staff scientists work closely with engineers and technicians to realize an instrument for a certain application. These highly experienced scientists will then later-on also operate the instruments. The Jülich Centre for Neutron Science JCNS has such

staff scientists located at the outstations at FRM II, ILL and SNS. However, these large scale facilities are way too expensive to be operated just for a small number of scientists. Beamtime is offered to external users from universities, research organizations (such as Max-Planck or Fraunhofer in Germany) and industry. In order for these users to obtain access to a scattering instrument, the user will obtain information from the internet on available instruments, contact the instrument scientist and discuss the planned experiments with the instrument scientist. Once a clear idea and strategy for an experiment has been worked out, the user will write a beamtime proposal where he describes in detail the scientific background, the goal of the planned experiment, the experimental strategy and the prior work. The facility issues a call for proposals in regular intervals, typically twice a year. The proposals received are distributed to members of an independent committee of international experts, which perform a peer review of the proposals and establish a ranking. Typically overload factors between 2 to 3 occur i. e. 2 to 3 times the available beam time is being demanded by external users. Once the best experiments have been selected, the beamtime will be allocated through the facility, where the directors approves the ranking of the committee, the beamline scientist schedules the experiments on the respective instrument and the user office sends out the invitations to the external users. Many facilities will pay travel and lodging for 1 up to 2 users per experiment. It is now up to the user to prepare the experiment as well as possible. If the experiment fails because it was not well prepared, it will be very difficult to get more beamtime for the same scientific problem. Typical experiments last between 1 day and up to 2 weeks. During this time lots of data will be collected which users take home and usually spend several weeks or months to treat the data and model it.

A typical scattering facility will run about 200 days a year with a few hundred visits of user from all over the world. This is also what makes research at large facilities so attractive to young scientists: early-on in their career they will learn to work in large international collaborations, get the opportunity to work on state-of-the-art high-tech equipment and learn to organize their research as efficient as possible. You have therefore chosen well to attend this Spring School!

Conclusion

This overview was meant to give a first introduction to scattering methods, give a climbse of the possibilities provided at current and future sources and outline the structure of the course. You can now look forward to interesting lectures, where many more details will be explained and you will learn the principles to enable you to successfully perform experiments at neutron and synchrotron radiation sources. Have lots of fun and success working with these powerful techniques!

References

[1] W. Friedrich, P. Knipping, M. von Laue, Interferenzerscheinungen bei Röntgenstrahlen, *Sitzungsberichte der Mathematisch-Physikalischen Klasse der Königlich-Bayerischen Akademie der Wissenschaften zu München* (1912) 303 - 322.

[2] W. H. Bragg, W. L. Bragg, The reflection of x-rays by crystals, *Proc. R. Soc. Lond.* **A88** (1913) 428 - 438.

[3] H. Geiger, E. Marsden, On a diffuse reflection of the alpha particles, *Proc. Roy. Soc.* **A82** (1909) 495 - 500.

[4] H. Geiger, E. Marsden, The laws of deflection of the particles through large angles, *Philosophical Magazine Series* **6** (1913) 25604 - 25623.

[5] E. Rutherford, The scattering of alpha and beta particles by matter and the structure of the atom, *Philosophical Magazine* **21** (1911) 669 - 688.

[6] J. Chadwick, Possible existence of a neutron, *Nature* **129** (1932) 312.

[7] J. Chadwick, The existence of a neutron, *Proc. Roy. Soc.* **A136** (1932) 692 - 708.

[8] http://www.atomicarchive.com/History/firstpile

[9] C. G. Shull, Early development of neutron scattering, *Nobel lecture* (1994) www.nobelprize.org.

[10] C. G. Shull, J. S. Smart, Detection of antiferromagnetism by neutron diffraction, *Physical Review* **76** (1949) 1256 - 1257.

[11] B. N. Brockhouse, Slow neutron spectroscopy and a grant enclass of the physical world, *Nobel lecture* (1994). www.nobelprize.org.

[12] R. R. Elder, A. M. Gurewitch et al., Radiation from Electrons in a Synchrotron, *Physical Review* **71** (1947) 829 - 830.

[13] www.XFEL.eu

[14] http://ess-scandinavia.eu/

[15] Y. Su, P. Link, et al., Antiferromagnetic ordering and structural phase transition in $Ba_2Fe_2As_2$ with Sn incorporated from the growth flux, *Physical Review B* **79** (2009) 064504.

[16] Y. Xiao, Y. Su, et al., Magnetic order in the $CaFe_{1-x}Co_xAsF$ (x = 0.00,0.06,0.12) superconducting compounds, *Physical Review B* **79** (2009) 060504.

[17] Y. Xiao, Y. Su, et al., Magnetic structure of $EuFe_2As_2$ determined by single-crystal neutron diffraction, *Physical Review B* **80** (2009) 174424.

[18] J. Herrero-Martín, V. Scagnoli, et al., Magnetic structure of $EuFe_2As_2$ as determined by resonant x-ray scattering, *Physical Review B* **80** (2009) 134411.

[19] S. Nandi, Y. Su, et al., Strong coupling of Sm and Fe magnetism in SmFeAsO as revealed by magnetic x-ray scattering, *Physical Review B* **84** (2011) 054419.

[20] P. J. Brown, T. Chatterji, et al., Magnetization distribution in the tetragonal phase of $BaFe_2As_2$, *Physical Review B* **82** (2010) 024421.

[21] Y. Xiao, Y. Su, et al., Field-induced spin reorientation and giant spin-lattice coupling in $EuFe_2As_2$, *Physical Review B* **81** (2010) 220406.

[22] S. Disch, The spin structure of magnetic nanoparticles and in magnetic nanostructures, *RWTH Aachen University, PhD* (2010).

[23] S. Disch, E. Wetterskog, et al., Quantitative spatial magnetization distribution in iron oxide nanocubes and nanospheres by polarized small angle neutron scattering, *New Journal of Physics* **14** (2012) 013025.
[24] S. Disch, E. Wetterskog, et al., Shape Induced Symmetry in Self-Assembled Mesocrystals of Iron Oxide Nanocubes, *Nano Letters* **11** (2011) 1651-1656.
[25] R. Mittal, L. Pintschovius, et al., Measurement of Anomalous Phonon Dispersion of $CaFe_2As_2$ Single Crystals Using Inelastic Neutron Scattering, *Physical Review Letters* **102** (2009) 217001.
[26] R. Mittal, R. Heid, et al., Pressure dependence of phonon modes across the tetragonal to collapsed-tetragonal phase transition in $CaFe_2As_2$, *Physical Review B* **81** (2010) 144502.
[27] R. Mittal, Y. Su, et al., Inelastic neutron scattering and lattice-dynamical calculations of $BaFe_2As_2$, *Physical Review B* **78** (2008) 104514.
[28] R. Mittal, S. Rols, et al., Phonon spectra in $CaFe_2As_2$ and $Ca_{0.6}Na_{0.4}Fe_2As_2$: Measurement of the pressure and temperature dependence and comparison with ab initio and shell model calculations, *Physical Review B* **79** (2009) 144516.
[29] R. Mittal, M. Zbiri, et al., Effects of magnetic doping and temperature dependence of phonon dynamics in $CaFe_{1-x}Co_xAsF$ compounds (x = 0, 0.06, and 0.12), *Physical Review B* **79** (2009) 214514.
[30] M. Zbiri, R. Mittal, et al., Magnetic lattice dynamics of the oxygen-free FeAs pnictides: how sensitive are phonons to magnetic ordering?, *Journal of Physics-Condensed Matter* **22** (2010) 8.
[31] R. Biehl, B. Hoffmann, et al., Direct Observation of Correlated Interdomain Motion in Alcohol Dehydrogenase, *Physical Review Letters* **101** (2008) 138102.